The *Fusarium graminearum* effector protease FgTPP1 suppresses immune responses and facilitates Fusarium Head Blight Disease

Martin Darino[†1], Namrata Jaiswal[†2], Reynaldi Darma[†1], Erika Kroll[1], Martin Urban[1], Youhuang Xiang[3], Moumita Srivastava[1], Hye-Seon Kim[4], Ariana Myers[2], Steven R. Scofield[2], Roger W. Innes[3], Kim E. Hammond-Kosack[1*], and Matthew Helm[2*]

† these authors contributed equally to this work

* co-corresponding authors

Present addresses: MS, Rajiv Gandhi Centre for Biotechnology, Thiruvananthapuram, Kerala, India; AM, Axbio Inc., Santa Clara, CA 95054

[1] Protecting Crops and the Environment, Rothamsted Research, Harpenden, Hertfordshire, AL5 2JQ, U.K.

[2] Crop Production and Pest Control Research Unit, U.S. Department of Agriculture-Agricultural Research Service (USDA-ARS), West Lafayette, IN 47907, U.S.A.

[3] Department of Biology, Indiana University, Bloomington, IN 47405, U.S.A.

[4] U.S. Department of Agriculture-Agricultural Research Service (USDA-ARS), National Center for Agricultural Utilization Research, Mycotoxin Prevention and Applied Microbiology Research Unit, Peoria, IL 61604, U.S.A.

*** Corresponding authors:** M. Helm, Email: Matthew.Helm@usda.gov; K. H-K, Email: kim.hammond-kosack@rothamsted.ac.uk

FUNDING

This research was supported by the United States Department of Agriculture, Agricultural Research Service (USDA-ARS) research project 5020-21220-014-00D, the U.S. Wheat and Barley Scab Initiative (award number 58-5020-0-013), and the USDA-National Institute of Food and Agriculture (NIFA) grant awarded to R. Innes and M. Helm (award number 2022-67013-38265). R. Darma is supported by a grant from the Biotechnology and Biological Sciences Research Council (BBSRC) (BB/X012131/1). Additional funding to support K. Hammond-Kosack, M. Urban and M. Darino has been provided by the BBSRC Institute Strategic Programme (ISP) Grants Designing Future Wheat (BBS/E/C/000I0250) and Delivering Sustainable Wheat (BB/X011003/1 and BBS/E/RH/230001B) and the BBSRC grant (BB/X012131/1). E. Kroll is supported by the BBSRC-funded South West Biosciences Doctoral Training Partnership (BB/T008741/1). The funding bodies had no role in designing the experiments, collecting the data, or writing the manuscript.

ABSTRACT

Most plant pathogens secrete effector proteins to circumvent host immune responses, thereby promoting pathogen virulence. One such pathogen is the fungus *Fusarium graminearum*, which causes Fusarium Head Blight (FHB) disease on wheat and barley. Transcriptomic analyses revealed that *F. graminearum* expresses many candidate effector proteins during early phases of the infection process, some of which are annotated as proteases. However, the contributions of these proteases to virulence remains poorly defined. Here, we characterize a *F. graminearum* endopeptidase, FgTPP1 (FGSG_11164), that is highly upregulated during wheat spikelet infection and is secreted from fungal cells. To elucidate the potential role of FgTPP1 in *F. graminearum* virulence, we generated *FgTPP1* deletion mutants (*ΔFgtpp1*) and performed FHB infection assays. Deletion of *FgTPP1* reduced the virulence of *F. graminearium* as assessed by spikelet bleaching. Infection with wild-type *F. graminearum* induced full bleaching in about 50% of the spikes at 10-11 days post infection, while this fraction was reduced to between 18 and 27% when using *ΔFgtpp1* mutants. Transient expression of green fluorescent protein (GFP)-tagged FgTPP1 revealed that FgTPP1 localizes, in part, to chloroplasts and attenuates chitin-mediated activation of mitogen-activated protein kinase (MAPK) signaling, reactive oxygen species production, and cell death induced by an autoactive disease resistance protein when expressed *in planta*. Notably, the FgTPP1 protein is conserved across the *Ascomycota* phylum, suggesting it may be a core effector among ascomycete plant pathogens. These properties make FgTPP1 an ideal candidate for decoy substrate engineering, with the goal of engineering resistance to FHB.

Keywords: wheat (*Triticum aestivum*), *Fusarium graminearum*, Fusarium Head Blight disease, protease, chloroplast, ROS, MAPK, cell death, pathogenesis, immune suppression

INTRODUCTION

Most fungal phytopathogens express and secrete a repertoire of proteins known as effectors during pathogenesis that modulate plant cell defense responses to facilitate infection and thus disease progression (Bentham et al. 2020). Once secreted, effectors can either be retained in the plant apoplast or translocated directly into host cells where they target multiple host proteins, thereby interfering with host cell-derived defense responses (Selin et al., 2016). To circumvent the immune-modulating activities of effectors, plants have evolved a two-tiered immune signaling network composed primarily of cell surface-localized and intracellular immune receptors (Chen et al. 2022; McCombe et al. 2022; Rhodes et al. 2022). Activation of cell surface-localized immune receptors by pathogen-associated molecular patterns (PAMPs) initiates an intracellular immune signaling cascade that includes, in part, the increased production of extracellular reactive oxygen species (ROS), up-regulation of defense-related gene expression, and activation of mitogen-activated protein kinase (MAPK) signaling (Chen et al. 2022; McCombe et al. 2022; Rhodes et al. 2022). In turn, fungal phytopathogens have evolved effectors that are capable of suppressing ROS generation and

accumulation as well as MAPK signaling (Bentham et al. 2020; Chen et al. 2022; Deng et al. 2022; Ngou et al. 2022; Rogers et al. 2024).

Translocated effectors secreted by phytopathogens are diverse in terms of their sizes and specific functions. In the case of bacterial phytopathogens, many effectors have been shown to function as proteases that target specific host proteins to inactivate them (Chandrasekaran et al. 2016; Jashni et al. 2015). For example, the AvrRpt2 protease from *Pseudomonas syringae* is secreted into Arabidopsis host cells, where it cleaves Arabidopsis RPM1-interacting protein 4 (RIN4) protein at two positions (Kim et al. 2005). RIN4 also interacts with proteins in the exocyst complex and appears to regulate callose deposition in response to AvrRpm1 (Kim et al. 2005; Redditt et al. 2019). Similarly, the cysteine protease AvrPphB from *P. syringae* pv. *phaseolicola* targets a family of serine/threonine receptor-like cytoplasmic kinases involved in regulating cell surface-mediated immunity, rendering these kinases inactive (Shao et al. 2003; Zhang et al. 2010). In Arabidopsis, cleavage of one of these kinases, PBS1, by AvrPphB activates the intracellular immune receptor, RPS5, which initiates a signal-transduction cascade culminating in resistance to *P. syringae* strains expressing AvrPphB (Ade et al. 2007; Shao et al. 2003; Simonich and Innes 1995). Importantly, investigating how the Arabidopsis PBS1-RPS5 immune signaling module is activated by the AvrPphB protease has enabled researchers to bioengineer new-to-nature disease resistance specificities against plant pathogens in Arabidopsis as well as crop plants (Carter et al. 2019; Helm et al. 2019; Kim et al. 2016; Pottinger et al. 2020).

The Ascomycete fungal pathogen, *Fusarium graminearum*, causes Fusarium Head Blight (FHB) disease in wheat (*Triticum* species), barley (*Hordeum vulgare*) and

other cereal crops, often causing premature senescence and blighting of wheat floral tissues (Armer et al., 2024a; Dean et al. 2012; Figueroa et al. 2018; Kanja et al. 2021). FHB is considered one of the most economically important fungal diseases of cereal grains, with estimated economic losses exceeding ~1 billion (USD) annually in direct and indirect effects (Figueroa et al. 2018; Nganje et al. 2004). In addition to reducing overall grain yields, FHB disease contaminates the remaining grain with sesquiterpenoid trichothecene mycotoxins such as deoxynivalenol (DON), which, in turn, affects grain marketability and threatens food safety (Figueroa et al., 2018; Hohn and Desjardins, 1992; Johns et al., 2022). *F. graminearum* employs a hemibiotrophic infection strategy to colonize different host structures such as wheat floral tissues and coleoptiles (Armer et al., 2024b; Brown et al. 2011; Mentges et al. 2020; Qiu et al. 2019). During the symptomless infection phase, unbranched hyphae spread on the exterior surfaces of the host and form appressoria-like infection cushion structures that enable direct penetration of the cell wall of wheat cells (Mentges et al. 2020; Qiu et al. 2019). Once established, the fungus develops bulbous biotrophic hyphae that branch and push into the host cell displacing the central vacuole (Qiu et al. 2019). Importantly, the plasma membrane of the invaded wheat cells remains intact, indicating that the early phases of infection are biotrophic (Brown et al. 2017; Qiu et al. 2019). During the later combined asymptomatic and symptomatic phases of disease development, *F. graminearum* develops extracellular hyphae to advance within and colonize the apoplastic environment (Brown et al. 2011; Qiu et al. 2019). Coincident with the appearance of disease symptoms, hyphae penetrate into adjacent wheat cells and this change is often accompanied by host cell death (Brown et al. 2011; Qiu et al. 2019).

The DON mycotoxin is required for successful traversing of the plasmodesmatal connections between wheat cells (Armer et al. 2024b). Collectively, fungal internal colonization and systemic spread through the wheat rachis results in bleached spikelets (Brown et al. 2012, 2017).

Similar to other plant pathogenic fungi, *F. graminearum* is predicted to secrete effector proteins during early phases of infection (Brown et al. 2012, 2017; Hao et al. 2020, 2023; Lu et al. 2016; Miltenburg et al. 2022). However, our general knowledge of how *F. graminearum* effector proteins contribute to plant pathogenesis remains limited. Nevertheless, several *F. graminearum* effectors have been identified and reported to have a functional role in fungal pathogenicity. For example, Jiang and colleagues (2020) showed that *F. graminearum* secretes an effector protein designated FgOSP24 (Orphan Secreted Protein 24) into the host cell cytoplasm where it subsequently interacts with and promotes the degradation of the SNF1-related kinase, TaSnRK1a. Recent work by Hao et al. (2023) identified a *F. graminearum* effector, FGSG_04563 (FgNls1), that is highly expressed during early phases of FHB disease development, localizes to plant cell nuclei, and interacts with wheat histone 2B (TaH2B). Importantly, deletion of *FgNls1* from *F. graminearum* reduces disease progression within wheat spikes. Host-induced silencing of *FgNls1* suppresses FHB disease development, indicating a functional role for FgNls1 in fungal pathogenesis (Hao et al. 2023). Similarly, two candidate *F. graminearum* effectors, ARB93B and FGSG_01831, have been shown to be expressed during the early stages of infection and to suppress cell surface-triggered immune responses, including PAMP-triggered reactive oxygen species production (Hao et al. 2019, 2020).

In addition to the aforementioned *F. graminearum* effectors, two candidate effector proteases have been identified that appear to contribute to *F. graminearum* virulence. Specifically, deletion of genes encoding a fungalysin metallopeptidase known as FgFly1 (FGSG_03467) and a subtilisin-like protease termed FgPrb1 (FGSG_00192) attenuates *F. graminearum* virulence and FHB disease progression in wheat spikes (Wang et al. 2022; Xu et al. 2020). Recent work by Xiong and colleagues (2024) identified five subtilisin-like proteases from *F. graminearum* (FgSLP1-5) that trigger cell death in *Nicotiana benthamiana*, Arabidopsis, and cotton (*Gossypium barbadense*). These cell death-inducing activities were independent of BAK1, SOBIR1, EDS1, and PAD4-mediated signaling. Importantly, *F. graminearum* mutants lacking two subtilisin-like proteases, FgSLP1 and FgSLP2, showed reduced fungal virulence in wheat, demonstrating FgSLP1 and FgSLP2 likely contribute to virulence (Xiong et al. 2024). Recently, Liu et al. (2024) identified a serine carboxpeptidase, FgSCP (FGSG_08454) that is expressed during early FHB disease development. Deletion of FgSCP inhibits fungal reproduction, alters vegetative growth, as well as reduces *F. graminearum* virulence and DON biosynthesis in wheat (Liu et al. 2024). Collectively, these studies highlight the important roles of *F. graminearum* proteases during pathogenicity. However, despite the importance of *F. graminearum* globally, host proteins thatare targeted by effector proteases from this fungus have yet to be identified. s.

To further understand how candidate secreted effector proteases from *F. graminearum* contribute to fungal virulence, we initially took a computational biology approach to identify the predicted secreted proteases present in the most recent *F. graminearum* genome annotation and identified one candidate protease, FGSG_11164

(FGRAMPH1_01G21371), that was highly expressed during floral wheat spike colonization (Brown et al. 2012, 2017; King et al. 2015, 2017a). FGSG_11164 encodes a putative trypsin precursor protein and, therefore, has been designated FgTPP1 (*Fusarium graminearum* Trypsin precursor protein 1). Here, we show that the predicted signal peptide from FgTPP1 is functional and facilitates secretion of FgTPP1 from fungal cells. Importantly, *F. graminearum* mutants lacking FgTPP1 expression (Δ*Fgtpp1*) showed a significantly slower disease progression and colonization of wheat spikes when compared to the wild-type *F. graminearum* PH-1, indicating that FgTPP1 contributes to fungal virulence. Agrobacterium-mediated transient expression of green fluorescent protein (GFP)-tagged FgTPP1 in *N. benthamiana* leaves revealed that FgTPP1 localizes, in part, to chloroplast stroma and attenuates chitin-mediated activation of mitogen-activated protein kinase (MAPK) signaling, reactive oxygen species production, and cell death induced by an autoactive disease resistance protein, demonstrating FgTPP1 suppresses multiple plant immune responses. Lastly, we show that the TPP1 protein is conserved in fungal species from different genera of the *Ascomycota* phylum suggesting a conserved role(s) for TPP1 in different plant-infecting fungi.

RESULTS

F. graminearum strain PH-1 expresses multiple candidate effector proteases during early wheat spikelet infection.

To identify putative effector proteases secreted by *F. graminearum,* we searched the most recent genome annotation of *F. graminearum* (YL1 version, NCBI GenBank number: PRJNA782099) for the terms ‘peptidase’ and ‘protease’ and screened this gene subset for the presence of signal peptides, which would suggest the putative proteases are secreted. This search identified 95 genes encoding putative secreted proteases. To further narrow this list, we selected genes that were upregulated during the early symptomless stages following *F. graminearum* infection of wheat spikes (at 3 and/or 7 days post-inoculation) (Brown et al. 2017). These stringent selection criteria identified seven candidate fungal proteases, of which six had been previously tested and shown not to be essential for virulence, at least when individually mutated (Table 1) (Wang et al. 2022; Xiong et al. 2024; Xu et al. 2020). Hence, we focused on functionally characterizing the remaining candidate protease, FGSG_11164 (FGRAMPH1_01G21371).

Analysis of the FGSG_11164 amino acid sequence with InterProScan indicated that this gene encodes a trypsin precursor protein (Figure 1A). We thus designated FGSG_11164 as *Fusarium graminearum* Trypsin precursor protein 1 (FgTPP1). FgTPP1 encodes a predicted 17-amino acid signal peptide sequence and a trypsin-like serine protease domain (amino acids 27-248) (Figure 1A). Further examination and *in silico* modeling of the FgTPP1 protein using AlphaFold2 showed that the protein has three predicted catalytic active sites, histidine-67 (His67), aspartic acid-112 (Asp112), and serine-208 (Ser208) as well as a putative substrate binding site consisting of aspartic acid-202 (Asp202), serine-224 (Ser224), and glycine-226 (Gly226) (Figure 1A and 1B). Intriguingly, FgTPP1 is also predicted to contain a chloroplast targeting peptide

sequence (amino acids 62-102), suggesting it may localize to chloroplasts (Figure 1A and 1B).

The predicted signal peptide of FgTPP1 confers secretion in yeast cells.

To test whether the predicted signal peptide of FgTPP1 is functional, we performed a yeast secretion trap assay (Zhou et al. 2020). This assay employs a *suc2* yeast mutant that is unable to grow on medium with sucrose as the sole carbon source (Zhou et al. 2020). We fused full length *FgTPP1*, including its signal peptide sequence, to a truncated *SUC2* gene lacking a signal peptide ($SUC2^{22\text{-}511}$), generating a pGAD-FgTPP1:$SUC2^{22–511}$ construct, which was subsequently transformed into a *suc2* yeast mutant. As a negative control, the truncated *SUC2* gene was fused to *FgTPP1* lacking its signal peptide sequence (pGAD-$FgTPP1^{\Delta SP}$:$SUC2^{22–511}$). A pGAD-$SUC2^{22–511}$ only construct was used as an additional negative control. As a positive control, we fused the *F. graminearum* effector FgOSP24, which was previously shown to be secreted (Jiang et al. 2020), to the truncated $SUC2^{22–511}$ gene and transformed this pGAD-FgOSP24:$SUC2^{22–511}$ construct into a *suc2* yeast mutant. As expected, *suc2* yeast mutants expressing either pGAD-$FgTPP1^{\Delta SP}$:$SUC2^{22–511}$ or pGAD-$SUC2^{22–511}$ were unable to grow on yeast synthetic dropout media (SD) supplemented with sucrose as the sole carbon source, indicating $FgTPP1^{\Delta SP}$ and SUC2 proteins are not secreted (Figure 2). Consistent with our hypothesis, *suc2* yeast mutants transformed with either pGAD-FgTPP1:$SUC2^{22–511}$ or pGAD-FgOSP24:$SUC2^{22–511}$ consistently grew on SD media supplemented with glucose or sucrose, demonstrating that the FgOSP24-SUC2 and FgTPP1-SUC2 fusion proteins are secreted (Figure 2). These data thus confirm

that the predicted signal peptide from FgTPP1 is indeed functional and confers secretion of FgTPP1 from fungal cells.

FgTPP1 contributes to fungal virulence.

Transcriptome data sets obtained from spatial and temporal analyses of the early symptomatic and asymptomatic phases of *F. graminearum* colonization of wheat spikes revealed that the *FgTPP1* gene is strongly induced during the first week of infection (Brown et al. 2017). To assess whether FgTPP1 contributes to fungal virulence, we used a homologous recombination strategy to replace the *FgTPP1* gene with a cassette expressing a bacterial gene conferring resistance to hygromycin B (Supplementary Figure S1A) (Catlett et al. 2003; King et al. 2017b). Primer combination P20 / P21 confirmed deletion of the *FgTPP1* coding sequence in two independent mutant strains (PH-1-Δ*Fgtpp1-1* and PH-1-Δ*Fgtpp1-3*) whilst primer combinations P16 / P17 and P18 / P19 confirmed replacement of the *FgTPP1* coding sequence by the hygromycin expression cassette (Supplementary Figure S1A and Supplementary Table S5). Both Δ*Fgtpp1* mutants displayed no observable defects in fungal morphology or radial growth when grown on Potato Dextrose Agar (PDA) plates, including under different stress conditions (Supplementary Figure S1B). Finally, no noticeable defects were observed in perithecia formation between the PH-1-Δ*Fgtpp1-1* mutant and wild-type *F. graminearum* PH-1 strain (Supplementary Figure S1C).

Next, we investigated whether FgTPP1 is involved in the infection process by performing fungal virulence assays using a top inoculation approach. In this assay, fungal spores of the PH-1-Δ*Fgtpp1-1* mutant and wild-type *F. graminearum* PH-1 strain

were inoculated into the 5th and 6th spikelets from the top of wheat spikes at anthesis of the susceptible wheat cultivar Bobwhite. Bleached spikelets below the point of inoculation were evaluated 12 days post-infection (dpi). The PH-1-Δ*Fgtpp1-1* mutant was able to infect the inoculated spikelets and systemically spread through the spike at a rate similar to that of wild-type *F. graminearum* PH-1 (Figure 3A). Consistent with the FHB symptoms, no differences in the number of diseased spikelets throughout the time-course and no statistically significant differences in the area under the disease progress curve (AUDPC) were observed between the PH-1-Δ*Fgtpp1-1* mutant and wild-type *F. graminearum* PH-1 strain (Figure 3A). To explore further potential virulence defects in the PH-1-Δ*Fgtpp1-1* mutant, we performed a second inoculation approach, which we refer to as the bottom inoculation assay. In brief, spores from either the PH-1-Δ*Fgtpp1-1,* PH-1-Δ*Fgtpp1-3*, or wild-type *F. graminearum* PH-1 were inoculated into the first two full-sized spikelets located at the base of a wheat spike at anthesis, and completely as well as partially bleached spikes were recorded at 10 dpi. In this approach, photobleaching of the spikelets may be a consequence of fungal spread and/or obstruction of the plant vascular tissue, which, in turn, may lead to cell death in wheat tissues above the inoculation point (Bai and Shaner 2004). Wild-type *F. graminearum* PH-1 caused approximately 50% of the spikes to be fully bleached at 10 dpi, while the PH-1-Δ*Fgtpp1-1* and PH-1-Δ*Fgtpp1-3* mutant strains induced fewer fully bleached spikes at this time point (18-27%) (Figure. 3B). To assess whether this difference was statistically significant, we tested whether the observed data fit a 1:1 ratio. While the data from the wild-type PH1 wild-type *F. graminearum* PH-1 infection fit this ratio, the

data from the mutant infections did not, indicating that these two *tpp1* mutants have reduced virulence (Figure 3B and 3C).

To test if partial bleaching of spikes compared to full bleaching was the consequence of either slower disease progression or developmental arrest, additional analyses were done. The rachis from each partially and fully bleached spike infected with either the wild-type *F. graminearum* PH-1 strain or the Δ*Fgtpp1-1* mutant was dissected into five segments and plated on synthetic nutrient agar (SNA). Fungal growth in the surrounding agar after 2 days revealed that the Fusarium hyphae were alive inside the infected rachises (Figure 3C). Fully bleached spikes infected with either Δ*Fgtpp1-1* mutant or wild-type *F. graminearum* PH-1 strain showed fungal growth on SNA for segment 1 that included the inoculation site and the adjacent segments 2 and 3 (Figure 3C). Rachis segments 4 and 5 towards the tip of the spike did not show the presence of fungal colonization, despite being fully bleached. In the case of the partially bleached spikes, rachis segments 1 and 2 showed the presence of fungus for all the spikes evaluated, whilst the presence of Fusarium hyphae in segment 3 was not always observed (Figure 3D). A lack of fungal colonization was evident in segments 4 and 5. However, rachis segments 4 and 5 inoculated either with the Δ*Fgtpp1-1* mutant or wild-type *F. graminearum* PH-1 strain remained either green or predominantly green with just some earlier symptoms of bleaching. Therefore, partially bleached spikes are most likely the consequence of slow disease progression rather than developmental arrest. In addition, the increased number of partially bleached spikes in both Δ*Fgtpp1-1* mutant strains in comparison to the wild-type *F. graminearum* PH-1 strain suggests that the mutants colonize the spikes more slowly (Figure 3B and 3D; Supplementary Figure 2).

Finally, we tested whether the slower spike colonization was a result of reduced production of the DON mycotoxin. DON concentrations were measured in wheat spikes infected with either Δ*Fgtpp1-1*, Δ*Fgtpp1-3,* or the wild-type *F. graminearum* PH-1 strain using the bottom inoculation approach at 10 days post-inoculation. DON values observed for the wild-type *F. graminearum* PH-1 strain were consistent with that of a previous report, when the top inoculation method was used (Cuzick et al. 2008). Significant differences were not observed between the Δ*Fgtpp1* mutants when compared to wild-type *F. graminearum* PH-1 strain, although there was a trend towards slightly reduced DON levels associated with both Δ*Fgtpp1* mutants (Supplemental Figure S1D). These results indicate that major changes in *in planta* DON levels were unlikely to be responsible for the slower colonization observed following inoculation with either Δ*Fgtpp1* mutants.

To confirm that the observed reduction in FHB disease progression in the bottom inoculation assay was a result of the absence of FgTPP1, the Δ*Fgtpp1-1* mutant was complemented with a copy of full-length *FgTPP1*, including its native promoter and terminator, thereby generating the complemented strain PH-1-Δ*Fgtpp1-1*::*TPP1*. The complementing copy of *FgTPP1* was inserted into a recently described neutral locus in *F. graminearum,* namely Target Site Integration (TSI) locus 1 (Darino et al. 2024). The TSI locus 1 allows target site integration of different cassettes without affecting either fungal virulence or fungal growth under different conditions. PCR amplification confirmed the insertion of a single copy of the cassette as primer combination P28 / P29 amplified the expected 6,123 base pair PCR product (Supplementary Figure S1E and Supplementary Table S5). The PH-1-Δ*Fgtpp1-1*::*TPP1* strain did not show observable

defects in radial growth or fungal morphology when grown under different stress conditions and, importantly, restored the defect in virulence observed with the PH-1-Δ*Fgtpp1-1* mutant (Figure 3B and Supplementary Figures 1B and 2). Collectively, these data demonstrate that FgTPP1 contributes to *F. graminearum* virulence in wheat spikes.

FgTPP1 accumulates within the stroma of chloroplasts.

Analysis of the FgTPP1 amino acid sequence using the deep learning program LOCALIZER (Sperschneider et al. 2017) revealed that FgTPP1 encodes a predicted chloroplast targeting sequence (CTS, amino acids 62-102). To test whether FgTPP1 is indeed targeted to chloroplasts, we fused FgTPP1 (without its signal peptide) to the N-terminus of Green Fluorescent Protein (GFP) and transiently co-expressed it in *N. benthamiana* with mCherry-tagged Rubisco small subunit transit peptide (RbcS-TP:mCherry), a chloroplast stroma marker protein (Helm et al. 2022; Nelson et al. 2007). Live-cell imaging using laser-scanning confocal microscopy of *N. benthamiana* epidermal cells revealed that FgTPP1:GFP partially localized to the chloroplast stroma as indicated by an overlap in the fluorescence signal from FgTPP1:GFP and RbcS-TP:mCherry (Figure 4A). As a control, we expressed free GFP with RbcS-TP:mCherry to exclude the possibility that the apparent chloroplast localization of FgTPP1:GFP was a result of free GFP or chlorophyll autofluorescence. The experiments showed that the fluorescence signal from free GFP did not significantly overlap with the fluorescence signal from the RbcS-TP:mCherry construct (Figure 4A). We next performed immunoblot analyses to assess protein accumulation and confirm the integrity of the FgTPP1:GFP protein. Intriguingly, these experiments revealed that the FgTPP1:GFP

fusion protein consistently produced multiple, distinct protein products, suggesting that the fusion protein may be cleaved prior to or following entry into chloroplasts (Figure 4B). To further confirm chloroplast localization of FgTPP1, we fused the mCherry fluorescent protein to FgTPP1 (FgTPP1:mCherry) and performed live-cell imaging on chloroplasts isolated from *N. benthamiana*. Confocal microscopy imaging of isolated chloroplasts revealed mCherry fluorescence signal in some, but not all, chloroplasts (Figure 4C). Taken together, our results demonstrate that FgTPP1 partially localizes to chloroplasts when transiently expressed in *N. benthamiana*.

FgTPP1 suppresses cell surface- and intracellular-mediated immune responses.

Most pathogen effectors function, at least in part, to suppress host immune responses. Prior to testing whether FgTPP1 can suppress immune signaling, we first confirmed that chitin enhances the accumulation of phosphorylated Mitogen-activated protein kinase (MAPK) protein, specifically the phosphorylation of MAPK3 and MAPK6, which has been linked to immune response signaling downstream of pathogen recognition (Jaiswal et al. 2022). *N. benthamiana* leaves transiently expressing free GFP were infiltrated with either deionized water (mock) or chitin, and at 0-, 5-, and 10-minutes following treatment, accumulation of phosphorylated MAPK3 and MAPK6 protein was assessed using immunoblot analyses with MAPK3/6 phospho-specific antibodies These experiments revealed an increase in phosphorylated MAPK3 and MAPK6 protein in response to chitin treatment when compared to the mock control, demonstrating that the increased accumulation of phosphorylated MAPK protein is indeed chitin-mediated (Figure 5A). To test whether FgTPP1 could attenuate chitin-

mediated MAPK signaling, we treated *N. benthamiana* leaves transiently expressing either free GFP or FgTPP1:GFP with chitin and assessed accumulation of phosphorylated MAPK3 and MAPK6 protein. These experiments revealed that expression of FgTPP1:GFP protein consistently suppressed the accumulation of phosphorylated MAPK3 and MAPK6 in response to chitin relative to the free GFP control (Figure 5B).

Several effectors from *F. graminearum* have been previously shown to suppress chitin-triggered reactive oxygen species (ROS) production (Hao et al. 2019, 2020). To test whether FgTPP1 could also suppress chitin-mediated ROS accumulation, we transiently expressed either free GFP or FgTPP1:GFP in *N. benthamiana* leaves. Plants were subsequently challenged with chitin and ROS production was monitored over time using a previously optimized luminol-based assay (Rogers et al. 2024). Expression of FgTPP1:GFP consistently attenuated chitin-mediated ROS accumulation when compared to the free GFP control (Figure 5C). Taken together, our results indicate that FgTPP1 suppresses multiple chitin-mediated immune responses.

Two previously studied effector proteins from *F. graminearum*, namely FgOSP24 and FgNLS1, have been reported to suppress BAX (Bcl-associated X)-induced cell death in *N. benthamiana*, and thus likely have a functional role in subverting host immune responses (Hao et al. 2023; Jiang et al. 2020). To test whether FgTPP1 can suppress cell death, we used an allele of the Arabidopsis disease resistance protein RPS5, RPS5^{D266E}, which constitutively activates cell death when transiently expressed in *N. benthamiana* (Ade et al. 2007). We fused FgTPP1 to the N-terminus of super Yellow Fluorescent Protein (sYFP) and cloned FgTPP1:sYFP into the dexamethasone-

inducible expression plasmid, pTA7001 (Qi et al. 2012; Vinatzer et al. 2006). We then transiently co-expressed RPS5^{D266E} with either FgTPP1:sYFP or empty vector (e.v.), and assessed for the suppression of RPS5^{D266E}-mediated cell death 16 hours post-dexamethasone induction. These experiments revealed that FgTPP1:sYFP consistently attenuated RPS5^{D266E}-triggered cell death when compared to the empty vector control (Figure 5D). Collectively, our data demonstrate that FgTPP1 attenuates cell surface-triggered and intracellular-mediated immune responses. Furthermore, the observation that FgTPP1 is secreted, localizes, in part, to chloroplasts, and suppresses immune responses when expressed inside plant cells indicates that FgTPP1 functions inside plant cells and may thus be translocated from the fungus into the host cell during infection.

TPP1 alleles and TPP1 protein haplotypes are conserved among plant infecting fungi of the *Ascomycota* phylum

To identify alleles of the *FgTPP1* gene in the *F. graminearum* global population, the nucleotide coding sequence of *FgTPP1* from the *F. graminearum* PH-1 strain was aligned to the nucleotide coding sequences of 28 *F. graminearum* isolates collected in 15 countries covering six continents (Supplementary Table S1). Seven alleles of the *FgTPP1* gene were identified (alleles 1 to 7) (Figure 6A). However, only two protein haplotypes were identified from these 7 alleles (Figure 6). Protein haplotype I is encoded by alleles 1 to 5 whilst protein haplotype F is encoded by alleles 6 and 7. The difference between the two protein haplotypes resides in amino acid residue 4, where haplotype I possesses an isoleucine whilst haplotype F possesses phenylalanine

(Figure 6B). This amino acid change resides within the secretion signal, but both protein haplotypes are predicted to be secreted as determined by SignalP v6.0 (Teufel et al. 2022). Approximately 85.7% of *F. graminearum* strains, including PH-1, have the protein haplotype I whereas only four recent European strains collected from western bordering countries, including France, Belgium, and Luxembourg, between 2002 and 2008 have protein haplotype F. Next, we calculated the pairwise dN/dS ratios to assess the evolutionary divergence across the nucleotide coding sequences of *FgTPP1* from the 28 *F. graminearum* isolates. The dN/dS ratios were close to zero for all sequences with a maximum ratio value of 0.01 ± 0.004 observed between the *F. graminearum* isolates pair TPP1_S5A and TPP1_KSU23473 (Supplementary Table S3). These results strongly indicate the *FgTPP1* gene is under purifying selection within this species. Taken together, our analyses revealed the TPP1 protein sequence is highly conserved among *F. graminearum* isolates collected from diverse geographic regions during the last 50 years, suggesting that it plays a central role in *F. graminearum* survival.

To evaluate the degree of sequence conservation of FgTPP1 in other fungal species, a BlastP search was conducted using the FgTPP1 protein sequence as the query. Homologs of FgTPP1 containing both a predicted secretion signal and a chloroplast transit peptide were identified not only in fungal species from the Fusarium genus, but also in fungal species belonging to different genera within the *Ascomycota* phylum (Figure 7 and Supplementary Tables S2 and S3). The FgTPP1 protein appears to be highly conserved (amino acid similarity values between 99 to 81%) in several plant pathogen species residing within the *Fusarium sambucinum* species complex including

F. culmorum, *F. pseudograminearum*, *F. sporotrichioides*, *F. langsethiae*, *F. venenatum* and *F. poae* (Armer et al. 2024a; Waalwijk et al. 2018). In addition, the FgTPP1 protein is also conserved in other plant pathogenic Fusarium species (similarity values between 87 to 71%) such as *F. equiseti*, *F. fujikuroi*, *F. verticillioides*, *F. oxysporum* and *F. tricinctum* that belong to different Fusarium species complexes (Figure 7 and Supplementary Table S2). Some Fusarium species such as *F. sarcochroum*, *F. torreyae*, *F. tricinctum* and *F. avenaceum* possess two copies of the TPP1 gene (Supplementary Table S2). Finally, FgTPP1 is also conserved (similarity values between 64 to 52%) in fungal species from different genera within the *Ascomycota* phylum (Supplementary Table S4). Most of these species have been classified either as plant pathogenic (*Alternaria alternata* and *Verticillium dahliae*) or plant endophytic (*Colletotrichum tofieldiae* and *Alternaria rosae*) (Figure 7 and Supplementary Table S4). Multiple copies of TPP1 homologs were also discovered in species residing in the Alternaria genus. While *A. panax* and *A. rosae* have 2 copies of *TPP1*, 3 copies were found in *A. alternata* and *A. burnsii*. The strong conservation of *TPP1* across a wide range of Ascomycete plant pathogens and endophytes suggests that TPP1 may play a conserved role(s) in plant colonization.

DISCUSSION

In this study, we examined the functional roles and immune suppressing properties of a putative effector protease from *F. graminearum*, FgTPP1, which was previously shown to be upregulated during early stages of wheat spike infection by *F.*

graminearum, suggesting that it plays a role in fungal colonization and infection of the wheat spike. Consistent with this, the virulence of Δ*Fgtpp1* mutants was reduced when compared to the wild-type *F. graminearum* PH-1 strain using a bottom inoculation method. In this infection assay, *F. graminearum* colonizes the wheat rachis and vascular tissue, thereby inhibiting nutrient and water transport to the systemic, non-infected spikelets, resulting in bleaching of the wheat spike (Bai and Shaner 2004). During the bottom inoculation method, we observed fully bleached spikes and curved awns during the onset of spikelet bleaching (spike discoloration), which may be used as an additional criterion to categorize infection severity. Furthermore, these symptomatic characteristics allowed us to distinguish between fully bleached and partially bleached spikes, thereby affording us the opportunity to more consistently phenotype FHB disease progression. It is worth noting the importance of the timepoint when the inoculated plants were evaluated. We have observed that disease symptoms in partially bleached spikes progress over time and most of the partially bleached spikes become fully bleached at 13 dpi. Earlier scoring times, i.e. before 10 dpi, did not generate data sets that were able to distinguish between the *ΔFgtpp1* mutants and the wild-type *F. graminearum* PH-1 strain, as most of the infected spikes were partially bleached. Under our conditions, the transition from partially to fully bleached spikes occurs very quickly, typically over a 1-to-2-day time window, thus making it rather challenging to count diseased spikelets accurately throughout this brief phase of the infection time course. Therefore, this brief phase affects the accuracy of the AUDPC values. Instead, we have observed that wheat spikes infected with wild-type *F. graminearum* PH-1 follow a 1:1 ratio (partially : fully bleached spikes) at 10 dpi. This ratio can be used to establish if the

ΔFgtpp1 mutants deviate from the frequencies of partially / fully bleached spikes observed for the PH-1 strain. In contrast to the bottom inoculation method, the top inoculation approach consists of counting the number of diseased spikelets below the inoculation point and is often reliable when there are significant differences between mutant and wild type *F. graminearum* strains such as the recently characterized cell wall stress tolerance *ΔKnr4* mutant (Kroll et al. 2025). However, distinguishing between an infected and uninfected wheat spikelet can be challenging using the top inoculation method, especially during the early stages of spikelet infection. Consequently, reduced virulence phenotypes are often difficult to reliably phenotype, especially when subtle. In our study, we did not observe a reduction in fungal virulence with the ∆*Fgtpp1-1* mutant when using the top inoculation method and the wheat cultivar 'Bobwhite'. Our results presented here are also inconsistent with that of Menke (2011) who, in a non-peer reviewed study, showed that a ∆*Fgtpp1* mutant strain exhibited a subtle reduction in fungal virulence using the top inoculation method and the wheat cultivar 'Norm'. Specifically, Menke (2011) reported that the number of diseased spikelets per infected spike with the wild-type *F. graminearum* PH-1 strain was 7.7 ± 0.3 while the number of disease spikelets per spike infected with the ∆*Fgtpp1* mutant was 7.2 ± 0.2, a 6% reduction in fungal colonization. Collectively, our experiments using different infection methods suggest that the bottom infection method is likely more sensitive to subtle virulence defects and could be used to further analyze *F. graminearum* mutants that do not show significant virulence defects using the top inoculation method.

Approximately seven predicted proteases, some of which are highly expressed during *in planta* fungal growth have been individually deleted in *F. graminearum*.

However, only one *F. graminearum* mutant (FGSG_00192; FgPrb1) showed a significant reduction in fungal pathogenicity (Xu et al. 2020). This result may suggest that either candidate proteases are not directly involved in fungal pathogenicity, or fungal proteases may be functionally redundant, and, therefore, single deletion mutants are not sufficient to produce a strong reduction in fungal pathogenicity. For example, single gene deletions of two subtilisin-like protease genes, *FgSLP1* (FGSG_00806) and *FgSLP2* (FGSG_03315), did not significantly affect fungal virulence in wheat spikes when compared to wild-type *F. graminearum* PH-1 strain (Xu et al. 2020). However, simultaneous deletion of both *FgSLP1* and *FgSLP2* resulted in a significant reduction in fungal virulence, indicating *FgSLP1* and *FgSLP2* are functionally redundant and complement each other during pathogenesis (Xiong et al. 2024). In addition to subtilisin-like proteases, *F. graminearum* expresses other putative proteases during *in planta* growth that attenuate plant defense responses, such as the serine carboxypeptidase FgSCP (FGSG_08454) (K. Liu et al. 2024). The FgSCP protease from *F. graminearum* suppresses cell death when transiently expressed in *N. benthamiana*, positively regulates the expression of DON biosynthesis, and plays a direct role in *F. graminearum* pathogenicity in wheat as well as maize (K. Liu et al. 2024). Similar to FgSCP1 and FgTPP1, the aspartic protease FolAsp, from *F. oxysporum f. sp. lycopersici*, was recently shown to inhibit hypersensitive response (HR)-like cell death as well as suppress PAMP-mediated ROS burst in *N. benthamiana* (Wang et al. 2023). Importantly, FolAsp is involved in *F. oxysporum* f. sp. *lycopersici* pathogenicity in tomato seedlings (Wang et al. 2023). The observation that *F. graminearum* expresses and secretes multiple proteases that suppress plant immunity suggests deleting additional,

functionally redundant proteases, in the Δ*Fgtpp1* mutant may further reduce fungal virulence.

Our finding that FgTPP1 localizes, in part, to the chloroplast stroma suggests *F. graminearum* may modulate chloroplast-mediated immune responses during fungal infection. It is worth noting that biosynthesis of the defense phytohormone salicylic acid (SA) occurs, in part, within chloroplasts and SA production is important for defense against biotrophic and hemibiotrophic pathogens (Ding and Ding, 2020; J. Liu et al. 2024). In addition to salicylic acid, chloroplasts also produce reactive oxygen species, which often function as signaling molecules to propagate immune responses against pathogens (Galvez-Valdivieso and Mullineaux, 2010; J. Liu et al. 2024). Considering the importance of SA production and ROS accumulation during plant-pathogen interactions, it stands to reason that downregulation of chloroplast functions could potentially interfere with production of defense signaling molecules (Kretschmer et al. 2020). Indeed, several filamentous fungal pathogens have evolved effector proteins that localize to chloroplasts to subvert chloroplast-derived defense responses (Figueroa et al. 2021; Littlejohn et al. 2021). For example, the wheat stripe rust pathogen *Puccinia striiformis* f. sp*. tritici* expresses and secretes the Pst_12806 effector inside host cells where it subsequently localizes to host chloroplasts and interacts with the chloroplast iron-sulfur protein, TaISP (Xu et al. 2019). The poplar rust fungus *Melampsora larici-populina* encodes three chloroplast-targeting proteins (CTP1, CTP2, and CTP3) that, similar to FgTPP1, contain chloroplast targeting sequences and localize to the stroma of chloroplasts in *N. benthamiana* (Petre et al. 2015, 2016). Although we hypothesize that the immune suppressing activities of FgTPP1 may be a result of its localization to

chloroplasts, our data does not rule out the possibility that FgTPP1 may function in the nucleo-cytosol to suppress immunity. Hence, future work will focus on testing whether the subcellular localization of FgTPP1 is important for its immune-suppressing activities, identifying host proteins from wheat that interact with this candidate effector protease, and what effect such interactions have on facilitating *F. graminearum* infection and FHB disease development.

One of the reasons we have been researching effector proteases from *F. graminearum* is the potential to bioengineer novel recognition specificities of such proteases using decoy substrates. Many wheat and barley cultivars encode for the nucleotide-binding leucine-rich repeat (NLR) disease resistance gene *AvrPphB response 1* (*Pbr1*), which mediates recognition of the AvrPphB protease from *Pseudomonas syringae* (Carter et al. 2019; Jaiswal et al. 2023). AvrPphB is known to target receptor-like cytoplasmic kinases (RLCKs) in subfamily VII, which includes PBS1, from Arabidopsis (Shao et al. 2003; Zhang et al. 2010). We have previously shown that the AvrPphB cleavage site within PBS1 can be replaced with cleavage sequences for other pathogen-secreted proteases, including viral proteases, which then confers recognition and resistance to the pathogens expressing those proteases, including soybean mosaic virus and turnip mosaic virus (Helm et al. 2019; Kim et al. 2016). By extension, it may be feasible to introduce genetic-based resistance to *F. graminearum* by bioengineering a barley and wheat RLCK such that, when proteolytically cleaved by FgTPP1, activates PBR1-mediated immunity. While there are no reported NLR-based resistance genes against *F. graminearum*, we predict such NLR-mediated immune responses will be effective at conferring resistance to this fungal pathogen. For

example, the tomato NLR immune receptor I2 was shown to confer recognition and resistance to *F. oxysporum* f. sp. *lycopersici* (Simons et al. 1998). A major goal for us going forward will be the identification of the preferred cleavage site sequence for FgTPP1, which would then enable us to generate decoy substrates that, when cleaved, would activate immune responses. If successful, the bioengineering of barley and wheat RLCK decoy proteins is expected to contribute to the development of improved crop protection strategies for *F. graminearum*. Importantly, we would expect such resistance to be quite durable, as *FgTPP1* is conserved among all sequenced *F. graminearum* genomes and the gene appears to be under purifying selection within the *F. graminearum* species, which indicates that it likely has a central role in the *F. graminearum* life cycle. Furthermore, the conservation of *Fgtpp1* across fungal plant pathogens from the Ascomycetes phylum suggests that it may be possible to bioengineer resistance to fungal plant diseases of many different crops using the same approach.

MATERIALS and METHODS

Strain, media, and culture.

Fusarium graminearum wild-type strain PH-1 (Cuomo et al. 2007) was used as the background strain to generate the Δ*Fgtpp1* mutant strains. The wild-type PH-1, PH-1-Δ*Fgtpp1* mutant strains, and the complementation strain PH-1-Δ*Fgtpp1-1*::*TPP1* were grown on synthetic nutrient agar (SNA; 0.1% KH_2PO_4, 0.1% KNO_3, 0.1% $MgSO_4$ x 7 H_2O, 0.05% KCl, 0.02% glucose, 0.02% saccharose, and 2% agar) under constant

ultraviolet and white light illumination. Conidiation was induced by adding 3 mL of TB3 liquid medium (0.3% yeast extract, 0.3% casamino acids, and 20% sucrose) to SNA plates containing 7-day old fungal mycelia. Conidia were harvested 2 days later in sterile water and stored at -80°C as described previously (Brown et al. 2011). *Escherichia coli* strain DH5α was used for plasmid construction. *E. coli* transformants were selected on Luria-Bertani (LB) agar supplemented with either 25 µg/mL gentamicin or 100 µg/mL ampicillin. Defects in radial growth in the mutant and complemented strains compared to PH-1 were evaluated under different stress conditions as previously described (Darino et al. 2024). Briefly, 25mL of half-strength Potato Dextrose Agar (PDA) were mixed with different stress inducing agents such as membrane stresses (Congo Red [50 µg/mL], Calcofluor [100 µg/mL], and 0.02% Tergitol) and salt stress (1M NaCl) and poured into squares plates. The strains were also evaluated on SNA. Three 10-fold serial dilutions were prepared from a water stock containing 10^6 fungal conidia/mL. Each spore dilution was spotted onto agar plates in 20µl droplets. Plates were incubated at room temperature (RT) under dark conditions for the entirety of the experiment. Photographs were taken at 2 days post inoculation (dpi). The experiment was repeated twice. Defects in perithecia induction and formation between the PH-1-Δ*Fgtpp1-1* mutant strain and PH-1 were evaluated on carrot agar medium following the protocol described by Cavinder et al. (2012). Photographs were taken 9 days after inoculation of the fungal strains on plates containing carrot agar. The experiment was repeated three independent times.

Plant growth conditions.

Seeds of *N. benthamiana* were grown in pots containing Berger Seed and Propagation Mix supplemented with Osmocote slow-release fertilizer (14-14-14) and maintained in a growth chamber with a 16:8 h photoperiod (light:dark) at 24°C in the light and 20°C in the dark, with average light intensities at plant height of 120 µmols/m^2/s.

Spring wheat cultivar 'Bobwhite' seedlings were grown in pots containing Rothamsted mix soils with 50% the standard fertilizer rate and maintained in a controlled environment room with a 16:8 h photoperiod (light:dark) under white-based LEDs with far-red addition (HelioSPEC R40F Flex, Sweden) with average light intensities of 300 µmols/m^2/s and 65% relative humidity. Temperatures during light/dark conditions were 20°C and 18°C, respectively (Darino et al. 2024).

Prediction of the FgTPP1 protein structure using AlphaFold2.

The protein structure of FgTPP1 (without the predicted signal peptide sequence) was predicted using the ColabFold v1.5.2: AlphaFold2 using MMseqs2 with default parameters as previously described (Mirdita et al. 2022; Rogers et al. 2024). The predicted protein structure with the highest confidence (pLDDT) score as determined by AlphaFold2 (i.e. ranked_0.pdb) was captured and visualized using ChimeraX-1.5 (Meng et al. 2023).

Yeast secretion trap assay for testing signal peptide function.

Secretion of different *F. graminearum* proteins was tested in yeast using the yeast secretion trap assay as previously described by Zhou and colleagues (2020) with

slight modifications. Briefly, secretion signals from FgTPP1 and FgOSP24 were predicted using SignalP v6.0 (Teufel et al. 2022). Full length coding sequences of *FgTPP1*, *FgOSP24*, and *FgTPP1* without the predicted secretion signal (*FgTPP1*$^{\Delta SP}$) were PCR-amplified using primer combinations P1 / P2, P3 / P4, and P5 / P2, respectively, using cDNA generated from wheat floral tissue infected with *F. graminearum* wild type strain PH-1 as the template. The resulting PCR products were cloned into the pDONR207 plasmid using a Gateway cloning approach (Invitrogen). Donor clones containing pDONR207-*FgTPP1*, pDONR207-*FgOSP24*, and pDONR207-*FgTPP1*$^{\Delta SP}$ were recombined with the destination vector pGAD-GW-SUC2$^{22\text{-}511}$ using the Gateway cloning system (Invitrogen) to generate the following constructs: pGAD-*FgTPP1*:SUC2$^{22–511}$, pGAD-*FgOSP24*:SUC2$^{22–511}$, and pGAD-*FgTPP1*$^{\Delta SP}$:SUC2$^{22–511}$. Each construct was transformed into a yeast sucrose invertase (*suc2*) mutant using a yeast transformation kit following the manufacturer's instructions (Yeast Transformation Kit, Sigma-Aldrich). The *suc2* mutant is unable to secrete the SUC2 protein and thus cannot grow on media containing sucrose (Suc) as the sole carbon source. Transformants were plated on yeast synthetic dropout media (SD) lacking tryptophan and leucine (-TL) supplemented with 2% glucose (Glu). The lack of tryptophan and leucine is to select positive transformants of the yeast *suc2* mutant containing the different constructs. Plates were incubated at 30°C for 3 days. Yeast transformants were verified by PCR amplification to determine the presence of the fusion proteins using the primer combination P6 and P7. Positive clones were inoculated into liquid SD-TL 2% Glu media and incubated at 30ºC overnight with slight agitation (180 rpm). Following overnight incubation, liquid cultures were adjusted to an optical density (OD)

at 600 nm (OD_{600}) of 1.0 and centrifuged at 4000 rpm for 2 minutes to remove the growth media. Yeast pellets were resuspended in sterile water and three 10-fold serial dilutions for each transformant were prepared. Five microliters of each dilution was spotted onto plates containing SD-TL supplemented with either 2% Glu or 2% Suc. Plates were incubated at 30°C for 4 days. Empty vector pGAD-GW-SUC2$^{22\text{-}511}$ was used as negative control. The experiment was repeated twice.

Deletion of *tpp1* and complementation in *F. graminearum*.

The ‘split-marker’ approach utilizing two overlapping DNA fragments was used to delete the *FgTPP1* gene from the *F. graminearum* PH-1 strain (Catlett et al. 2003; King et al. 2017b). Briefly, two plasmids, pEK01 and pEK02, were designed to delete *FgTPP1*. The vector pEK01 contained a 1,000 base pair fragment upstream of the start codon of the *FgTPP1* gene (P_{TPP1}) followed by a partial sequence of the hygromycin B resistance cassette ($Hyg_{1\text{-}761}$). P_{TPP1} was PCR-amplified from *F. graminearum* PH-1 genomic DNA using primers P8 and P9, whilst the $Hyg_{1\text{-}761}$ fragment was PCR-amplified from the pHyg1.4 vector using primers P10 and P11 (Urban et al. 2003). The vector pEK02 contained a fragment of the hygromycin B resistance cassette ($Hyg_{296\text{-}1027}$) followed by a 1,000 base pair fragment of the terminator region of *FgTPP1* downstream of the stop codon (T_{TPP1}). Primers P12 and P13 were used to PCR-amplify T_{TPP1} from PH-1 genomic DNA whilst primers P14 and P15 were used to PCR amplify the fragment $Hyg_{296\text{-}1027}$ from the pHyg1.4 vector. Gibson assembly was used to ligate the PCR fragments (P_{TPP1} with $Hyg_{1\text{-}761}$ and $Hyg_{296\text{-}1027}$ withT_{TPP1}) into the pGEM-T Easy vector to generate plasmids pEK01 and pEK02, respectively. The two plasmids share a 466 bp

overlapping region of the Hyg cassette to allow recombination during the transformation step.

To proceed with the transformation step, PCR products containing the P_{TPP1}-Hyg_{1-76} and $Hyg_{296-1027}$-T_{TPP1} were PCR-amplified using HotStart polymerase and primer combinations P8 / P11 and P14 / P13, respectively. Then, 5 µL aliquots of 2 µg/mL from each PCR product were combined and used to transform 1×10^8 protoplasts generated from *F. graminearum* PH-1 according to the protocols described by Hohn and Desjardins (1992) and King et al. (2017b). Transformants were selected on regeneration media (0.2% yeast extract, 0.2% casein-hydrolysate (N-Z-Amine A), 0.7% agarose and 0.8 M sucrose) containing 75 µg/mL hygromycin. Well-spaced transformants were selected using sterile wooden toothpicks and transferred to 6-well plates containing SNA with 75 µg/mL hygromycin. To extract genomic DNA, transformants were grown on YPD broth containing 75 µg/mL Hyg B and DNA was extracted according to the method described by Rudd et al. (2010). PCR diagnostic tests were performed to confirm the correct insertion of the Hyg cassette into the TPP1 locus (primer combinations: P16 / P17 and P18 / P19) and to test for *FgTPP1* coding sequence replacement (primer combination P20 / P21) (King et al. 2017b).

The Δ*Fgtpp1-1* mutant was complemented with the coding sequence of *FgTPP1* at the TSI locus 1 (Darino et al. 2024). A DNA fragment containing the *FgTPP1* coding sequence, including the promoter and terminator regions of *FgTPP1* (P_{tpp11}-*TPP1*-T_{tpp1}) was PCR-amplified from genomic DNA of PH-1 using primer combination P22 and P23. The PCR product was cloned into the Fg vector as previously described (Darino et al. 2024). The Fg vector contains a fragment of the geneticin resistance cassette followed

by the right border (RB) of the TSI locus 1 (*geneticin*$_{1\text{-}664}$-RB). Between the RB and the partial sequence of the geneticin cassette, there is a cloning site adapted to the Golden Gate cloning approach (Engler et al. 2009). Integration into the TSI locus 1 was accomplished following an adaptation of the split-marker approach (Darino et al. 2024). Briefly, a PCR product containing the partial fragment of the geneticin resistance cassette followed by the P$_{tpp1}$-*TPP1*-T$_{tpp1}$ region and the RB of the TSI locus 1 (*geneticin*$_{1\text{-}664}$-P$_{tpp1}$-*TPP1*-T$_{tpp1}$-RB) was PCR-amplified from the Fg vector using primer combination P24 and P25. A second PCR product containing the left border (LB) of the TSI locus 1 followed by the split fragment of the geneticin resistance cassette (*geneticin*$_{795\text{-}128}$) was amplified from the pJET-LB-geneticin vector using primer combination P26 and P27. Both PCR products possess an overlapping region of 536 bp to allow homologous recombination. The PCR products were adjusted to a final concentration of 2 µg/µL. Finally, 5 µL of each PCR product was aliquoted and mixed. The mixture of PCR products was used to transform *F. graminearum* protoplasts prepared from the PH-1-Δ*Fgtpp1-1* mutant following the protocol described above. Transformants were selected on SNA plates containing 75 µg/mL of geneticin. To test for single insertion of the expression cassette into the TSI locus 1, a diagnostic PCR spanning from outside the recombination region was performed using primer combination P28 and P29. A transformant with an amplicon of 6,123 bp was selected as the positive transformant. Primers used in this study are listed in Supplementary Table S5.

FHB virulence assays.

The susceptible spring wheat cultivar ‘Bobwhite’, sourced from the International Maize and Wheat Improvement Centre (CIMMYT, Mexico), was inoculated at anthesis following the top inoculation approach as previously described by Wood et al. (2020) with slight modifications. Briefly, two spikelets per wheat spike were inoculated, using 4 to 7 plants per fungal strain and only the first spike per plant. The 14th and 15th spikelets, counting up from the bottom, were point-inoculated with 5µL of 1x10^{5} conidia/mL of either PH-1-Δ*Fgtpp1-1* or wild-type *F. graminearum* PH-1. As a control, wheat cv. ‘Bobwhite’ plants were inoculated with sterile, deionized water. Inoculated wheat plants were incubated under high humidity conditions (above 80%) for 48 hours, with an initial 24 hours in the dark. Fusarium Head Blight disease was scored by counting the number of infected spikelets below the point of inoculation every 2 days until 12 days post-inoculation. Area under the disease progress curve (AUDPC) analysis was used to quantify statistical differences between the mutant and PH-1 according to Schandry (2017). The AUDPC values were calculated for each spike infected with PH-1-Δ*Fgtpp1-1* or PH-1. Then, AUDPC average values for PH-1-Δ*Fgtpp1-1* and PH-1 were calculated and significant differences between PH-1-Δ*Fgtpp1-1* mutant and PH-1 were calculated using a t test with $p< 0.05$.

A bottom-inoculation approach was also performed to assess the virulence of the PH-1-Δ*Fgtpp1* mutants and PH-1-Δ*Fgtpp1-1*::*TPP1* complementation strains compared to wild-type PH-1. This approach is an adaptation of a previously described protocol (Seong et al. 2005). The 3rd and 4th full sized spikelets from the bottom of the wheat spike were inoculated, one spike per plant, and typically 15 plants per fungal strain. Four independent replicates were performed. In each replicate, a similar number of

plants were inoculated with each fungal strain (typically 10 to 14) always timed with plant anthesis. The two spikelets at the base were point-inoculated with 5µL of $5x10^4$ conidia/mL of either PH-1-Δ*Fgtpp1-1,* PH-1-Δ*Fgtpp1-3*, PH-1-Δ*Fgtpp1-1*::*TPP1*, or PH-1. Inoculated plants were incubated as described above. Between 10- and 11-days post-inoculation and depending upon the disease severity per infection batch, wheat spikes were classified as either completely bleached (wherein all the spikelets were found to be bleach and the awns spread out) or partially bleached (wherein some but not all the spikelets were bleached, and most awns remained upright). A goodness of fit test was performed to test if the observed frequencies of fully bleached / partially bleached spikes for each fungal strain were the same or different. The experiment was repeated at least four independent times. Images were captured using Olympus OM-D E-M10 fitted with a M.Zuiko 30mm F3.5 macro lens.

Fungal detection from infected spikes.

Fully beached and partially beached spikes infected either with PH-1-Δ*Fgtpp1-1* or wild-type *F. graminearum* PH-1 strain were harvested at 10 dpi. The rachis from each infected spike was dissected into five segments. The rachis segments were surface sterilized by fully submerging the segments into a solution containing 0.6 % bleach and 0.02 % Tween-20 for 15 min. The segments were then washed three times with sterile water. The five segments belonging to the same rachis were plated on SNA containing 15 µg/ml of gentamycin to inhibit bacterial growth. The plates were incubated at room temperature under constant UV light for 2 days to allow the fungus inside the rachis to grow and spread into the neighboring agar. Images were captured as

described above. Three fully bleached and three partially bleached spikes from each fungal strain were assessed, with three uninfected rachises serving as mock controls.

DON mycotoxin measurements.

DON mycotoxin concentrations within wheat spikes infected either with the PH-1-Δ*Fgtpp1* mutant strains or wild-type *F. graminearum* PH-1 were assessed using the Deoxynivalenol (DON) Plate Kit (Beacon Analytical Systems, Inc., US). Briefly, the bottom part (8 spikelets from the base and its corresponding rachis segments) of bottom-inoculated wheat spikes infected with either wild-type *F. graminearum* PH-1 or the PH-1-Δ*Fgtpp1* were collected at 10 days post-inoculation and frozen in liquid nitrogen. Three independent spikes per strain were individually grounded to a fine powder. Five volumes of sterile water were added to the ground tissue. Then, the solution was mixed by vortexing, incubated at 30°C for 30 minutes, and the supernatant was collected after centrifugation at maximum speed (12,000 rpm). The supernatant was 500-fold diluted and 50 µl of this diluted supernatant was mixed with 50 µl of the enzyme conjugate following the protocol described by the manufacturer. Three independent mock-inoculated wheat spikes were also included as a negative control. A calibration curve using different DON concentrations was used to determine the DON parts per million (ppm) for each wheat spike. The experiment was repeated twice. Each replicate consisted of 12 plants where three spikes, one spike per plant, were inoculated with the different fungal strains. Mock values were reported as < 0.2 ppm as values were outside the lowest calibrator from the standard curve. An ANOVA test followed by

Tukey post-hoc test was performed to calculate significant differences between the Δ*Fgtpp1* mutants and wild-type *F. graminearum* PH-1 strain (p value < 0.05).

Generation of plant expression constructs.

The RPS5^{D266E}:myc and RbcS-TP:mCherry constructs have been described previously (Helm et al. 2022; Qi et al. 2012).

To generate the FgTPP1:GFP and FgTPP1:mCherry constructs, we used the Golden Gate protocol as previously described by Lampropoulos et al. (2013). Briefly, the *FgTPP1* open reading frame, without the predicted signal peptide and the stop codon, was PCR-amplified using primer combination P30 and P31 using cDNA isolated from wheat floral tissue infected with PH-1 as the template. The resulting PCR fragments were purified and combined in a single Golden Gate reaction with the destination vector pGGZ001 for *in planta* expression. The pGGZ001 plasmid contains a 35S promoter, Ω-element (protein expression enhancer), UBQ10 terminator, HygR resistant cassette and either mCherry or GFP as C-terminus tags. The resulting constructs were sequence confirmed and subsequently designated as FgTPP1:GFP (pGGZ001-35s-Ω-element-*FgTPP1*:GFP-UBQ10t-HygR) and FgTPP1:mCherry (pGGZ001-35s-Ω-element-*FgTPP1*:mCherry-UBQ10t-HygR). A free GFP construct (pGGZ001-35s-Ω-element-*GFP*-UBQ10t-HygR) was also generated using the aforementioned Golden Gate protocol.

To generate the FgTPP1:sYFP construct, the *FgTPP1* open reading frame (without the signal peptide sequence) was synthesized by TWIST Biosciences with codon optimization for expression in *N. benthamiana* and cloned into pTWIST-Kan by

the service provider. This ORF was then PCR-amplified with *attB*-containing primers. The resulting PCR fragments were purified and recombined into the Gateway entry vector, pBSDONR(P1-P4) (Qi et al. 2012) using BP Clonase II (Invitrogen) and the resulting construct was designated pBSDONR(P1-P4):*FgTPP1*. The pBSDONR(P1-P4):*FgTPP1* plasmid was mixed with the pBSDONR(P4r-P2):*sYFP* (Qi et al. 2012) plasmid and the Gateway-compatible expression vector pTA7001 (Vinatzer et al. 2006). Plasmids were recombined by the addition of LR Clonase II (Invitrogen). The resulting construct was designated pTA7001:*FgTPP1*:sYFP. All constructs were sequence-verified for proper sequence and reading frame.

Agrobacterium*-mediated transient expression in *Nicotiana benthamiana.

Transient protein expression assays were performed as previously described with minor modifications (Helm et al. 2022). Briefly, the constructs described above were mobilized into *Agrobacterium tumefaciens* GV3101 (pMP90) and grown on Luria-Bertani (LB) media plates supplemented with 25 µg/ml of gentamicin sulfate and 50 µg/ml of kanamycin for two days at 30°C. Cultures were prepared in liquid LB media supplemented with the appropriate antibiotics and were shaken overnight at 30°C on an orbital shaker. Following overnight incubation, cells were pelleted by centrifuging at 3000rpm for 3 minutes at room temperature. For confocal microscopy and immunoblot analyses, bacterial pellets were resuspended in 10 mM $MgCl_2$, adjusted, and mixed to an OD_{600} of 0.3 for each strain, and incubated with 100 µM of acetosyringone for 3-4 hours at room temperature. For the suppression of HR-like cell death assay, bacterial pellets of FgTPP1:sYFP and $RPS5^{D266E}$:myc were resuspended in 10 mM $MgCl_2$,

adjusted to an OD_{600} of 0.3 and 0.15, respectively, and incubated with 150 µM of acetosyringone for 3 hours at room temperature. All bacterial suspensions were infiltrated into the abaxial side of *N. benthamiana* leaves using a needless syringe. For pTA7001-based constructs, which are dexamethasone-inducible, gene expression was induced approximately 48 hours post-agroinfiltration by spraying leaves with 50 µM dexamethasone.

Confocal microscopy.

Confocal microscopy of *N. benthamiana* epidermal cells was performed twenty-four hours post-agroinfiltration using a Zeiss LSM880 Axio Examiner upright confocal microscope with a Plan Apochromat 20x/0.8 objective. Fluorescence from the GFP-tagged protein fusions was excited using a 488-nm argon laser and detected between 525-nm and 550-nm. Fluorescence from the mCherry-tagged constructs was excited with a 561-nm helium-neon laser and detected between 565-nm and 669-nm. All confocal micrographs shown are of single optical sections and processed using the Zeiss Zen Blue Lite program (Carl Zeiss Microscopy).

Immunoblot analyses.

N. benthamiana leaves transiently expressing the epitope-tagged constructs were harvested 24 or 48 hours following agroinfiltration, flash frozen in liquid nitrogen, and total protein extracted as previously described by Helm et al. (2022) for immunoblot analyses. Ten microliters of isolated total protein were separated on a 4-20% Tris-glycine stain free polyacrylamide gel (Bio-Rad) at 170 V for one hour in 1X

Tris/glycine/SDS running buffer. Total proteins were transferred to nitrocellulose membranes (GE Water and Process Technologies). Membranes were washed with 1X Tris-buffered saline (50 mM Tris-HCl, 150 mM NaCl, pH 7.5) solution supplemented with 0.1% Tween20 (TBST) and blocked in 5% skim milk (w/v) (Becton, Dickinson & Company) for at least 1 hour at room temperature. Proteins were detected with horseradish peroxidase (HRP)-conjugated anti-GFP (1:5,000; Miltenyi Biotec) antibodies for one hour at room temperature. Membranes were washed three times with 1X TBST solution and subsequently incubated with Clarity Western ECL (Bio-Rad) substrate solution for 5 minutes. Imaging of immunoblots was performed with an ImageQuant 500 CCD imaging system.

Chloroplasts isolation.

Chloroplast isolation was performed as previously described with slight modifications (Petre et al. 2016). *N. benthamiana* leaves transiently expressing the indicated epitope-tagged constructs were harvested 24 hours following agroinfiltration, cut into 1 mm^2 pieces, and incubated in 20 mL of cold isolation buffer (IB) (400 mM sorbitol, 50 mM of HEPES KOH 8M, 2 mM EDTA, and 1 mM $MgCl_2$) for 15 minutes on ice. Leaf pieces were homogenized with a PT 1200 C Polytron homogenizer (3 × 5 s full speed), and the lysate was immediately filtered through doubled Miracloth to remove cell debris. The filtrate was collected in 50 mL conical tubes and centrifuged at 3000 rpm for 10 minutes at 4°C. The pellet containing the organelles was resuspended in 400 µl of ice-cold isolation buffer, and chloroplasts were isolated by centrifugation on a Percoll gradient (1 mL of 80% v/v Percoll / IB and 3 mL of 40% v/v Percoll/IB in a 10 mL conical

tube) at 4500 rpm for 10 minutes at 4°C. Intact chloroplasts were collected from the bottom layer and subsequently used for laser scanning confocal microscopy.

MAP kinase (MAPK) activity assay.

Suppression of chitin-induced MAPK activation in *N. benthamiana* was performed as previously described with slight modifications (Jaiswal et al. 2022). Briefly, *N. benthamiana* leaves transiently expressing either free GFP or GFP-tagged TPP1 (FgTPP1:GFP) were infiltrated with either nuclease free water (mock treatment) or chitin hexamer dissolved in nuclease free water (5 µg/mL; Accurate Chemicals & Scientific Corporation). Leaf discs (10 mm diameter) were harvested and frozen in liquid nitrogen at 0-, 5-, and 10-minutes following mock or chitin infiltration. Total protein was extracted as described above. Proteins were detected using HRP-conjugated anti-GFP (1:5,000; Miltenyi Biotec), anti-plant actin (1:5000; Abbkine), or anti phospho-P42/44 MAPK (1:5000; Cell Signaling Technology), which detects phosphorylated MPK3 and MPK6. Membranes were washed three times with 1X TBST solution and subsequently incubated with Clarity Western ECL (Bio-Rad) substrate solution for 5 minutes. Imaging of immunoblots was performed with an ImageQuant 500 CCD imaging system. Experiments were performed at least three independent times with similar results.

Luminol-based reactive oxygen species (ROS) assay in *N. benthamiana.*

Suppression of ROS production in *N. benthamiana* was performed as previously described using a luminol-based chemiluminescence assay (Jaiswal et al. 2022; Rogers et al. 2024). *N. benthamiana* leaf discs (5 mm diameter) transiently expressing either

free GFP or FgTPP1:GFP were harvested two days post-agroinfiltration using a cork borer, gently washed three times in nuclease free water, and incubated overnight in sterile water in a 96-well OptiPlate™ microplate (Perkin Elmer). The following day, the deionized water was replaced with chitin elicitation solution (luminol [30 µg/mL], horseradish peroxidase [20 µg/mL], chitin hexamer [5 µg/mL] (Accurate Chemicals & Scientific Corporation), and nuclease-free water) and ROS production was monitored by chemiluminescence for 40 minutes in a microplate reader (Tecan Infinite M200 Pro). Experiments were performed at least three independent times with similar results.

Cell death suppression assay.

Forty-eight hours following agroinfiltration with either empty vector (e.v.), FgTPP1:sYFP, or RPS5^{D266E}:myc, *N. benthamiana* leaves were sprayed with 50 µM dexamethasone supplemented with 0.02% Tween20 (to induce expression of both RPS5^{D266E}:myc and FgTPP1:sYFP). At 16 hours post-transgene induction, *N. benthamiana* leaves were assessed for cell death and photographed under white and ultraviolet (UV) light. Experiments were performed at least three independent times with similar results.

TPP1 sequence analysis from *F. graminearum* global populations, dN/dS analysis, and phylogenetic analyses.

Haplotype analysis of FgTPP1 nucleotide sequences from *F. graminearum* isolates was conducted according to Darma (2024). In brief, *FgTPP1* nucleotide sequences from *F. graminearum* isolates available in the NCBI database were extracted

using BLAST+ v2.9.0+ (Camacho et al. 2009) and parsed into a FASTA fasta file using 'BLASTtoGFF_multiple.py' (DOI:10.5281/zenodo.13651118). FgTPP1 coding sequences from 28 *F. graminearum* isolates tested in this study are listed in the Supplementary File S1. *FgTPP1* sequences were aligned using Geneious 10.2.3 alignment with the Blosum62 cost matrix. Introns from those sequences were trimmed to generate coding sequences of *FgTPP1* from global populations. Allele networks from *FgTPP1* coding sequences were generated with POPart v1.7 (Leigh and Bryant, 2015) using minimum spanning network setting.

Pairwise dN/dS ratios were calculated using MEGA11 (Tamura et al. 2021) to assess selection pressure on the *FgTPP1* gene. The Tamura-Nei model (Tamura and Nei, 1993) was applied to account for transition/transversion bias, and dN/dS ratios were estimated with standard errors calculated via 1,000 bootstrap replicates. A ratio < 1 was interpreted as purifying selection, while > 1 indicated positive selection.

TPP1 protein sequences from *Fusarium* sp. and other fungi were extracted with BlastP. Multiple hits representing TPP1 homologs from different *Fusarium* species complexes were selected for further analysis. In addition, hits from other fungi, excluding *Fusarium* species, predicted as trypsin or serine protease with the minimum max score 243, were extracted for further analysis. TPP1 protein sequences from *Fusarium* species and other fungi were aligned using Geneious 10.2.3 alignment as described previously. An amino acid alignment of TPP1 proteins from *Fusarium* sp. and other fungi is available in Supplementary file S2. IQ-Tree 2.2.2.6 (Kalyaanamoorthy et al. 2017; Nguyen et al. 2015) was used to identify the best amino acid substitution model from the TPP1 amino acid sequence alignment and was used to generate a

maximum likelihood tree using 10,000 bootstrap replicates. In addition, a Bayesian inference tree was also generated to support the maximum likelihood tree using MrBayes 3.2.6 (Huelsenbeck and Ronquist, 2001) with the following settings: rate matrix (fixed) WAG, rate variation gamma, gamma categories 4, chain length 1,000,000, heated chains 4, heated chain temperature 0.2, subsampling frequency 10,000, burn-in length 100,000, and random seed 16,291. Finally, Figtree 1.4.4 (Rambaut 2018) was used to refine the appearance of the phylogenetic tree.

ACKNOWLEDGEMENTS

We thank Dr. Tesfaye Mengiste (Purdue University) for access to the microplate reader for the ROS suppression assays. We would also like to thank Dr. Terri Cameron for technical assistance, Dr. Ariel Sturgill-Helm for critical reading of the manuscript, and the Purdue University Imaging Facility for access to the Zeiss LSM880 Axio Examiner upright confocal microscope. The authors would also like to thank Dr. Fiona Doohan (University of Dublin, Ireland) for providing the pGAD-SUC2$^{22\text{-}511}$ plasmid and the *suc2* yeast mutant, Silvia Melina Velasquez for her technical assistance with the violin plots, Fiona Gilzean and the facilities team at Rothamsted Research for preparing and maintaining the various growth rooms used in this study whilst major refurbishment of the containment facilities were in progress. All experiments involving *F. graminearum* strain PH-1 and isogenic transformants were conducted in biological containment facilities under UK Defra license number 101948/198285. All opinions expressed in this paper are the authors' and do not necessarily reflect the policies and views of USDA.

Mention of trade names or commercial products in this publication is solely for the purpose of providing specific information and does not imply recommendation or endorsement by the U.S. Department of Agriculture. USDA is an equal opportunity provider and employer.

FIGURES and TABLES

Table 1. Summary of the candidate effector proteases expressed during early wheat spikelet infection.

Gene ID	Amino Acids	Signal peptide	Predicted annotation	Reference
FGSG_00192 (FgPrb1)	533	Yes (1-15)	Cerevisin precursor protein	Xu et al. 2020
FGSG_00806 (FgSLP1)	413	Yes (1-20)	Subtilisin-like peptidase	Xu et al. 2020 Xiong et al. 2024
FGSG_03315 (FgSLP2)	411	Yes (1-20)	Subtilisin-like peptidase	Xu et al. 2020 Xiong et al. 2024
FGSG_08012	390	Yes (1-18)	Proteinase T precursor protein	Xu et al. 2020
FGSG_11164	252	Yes (1-17)	Trypsin precursor protein	This study
FGSG_11472	875	Yes (1-17)	Subtilisin-like peptidase	Xu et al. 2020
FGSG_03467 (FgFly1)	631	Yes (1-23)	Fungalysin metallopeptidase	Wang et al. 2022

Figure 1. Schematic illustration and predicted protein structure of FgTPP1 (FGSG_11164). A, Schematic representation of the *F. graminearum* candidate effector protease FgTPP1 including the putative signal peptide (SP; aa 1-17) sequence and the predicted trypsin-like serine protease (Tryp_SPc; aa 27-248) domain. The predicted chloroplast targeting motif (aa 62-102) is indicated in green. Putative catalytic active sites (His-67, Asp-112, and Ser-208) are indicated by red triangles and predicted substrate binding sites (Asp-202, Ser-224, and Gly-226) are indicated by white squares. Numbers delineate amino acid positions. **B,** The predicted three-dimensional protein structure of FgTPP1 as determined by AlphaFold2. The predicted trypsin-like serine protease domain is indicated in light blue, the chloroplast targeting motif is indicated in green, and the putative catalytic residues are indicated in red. N-term: amino terminus.

Figure 2. The FgTPP1 protein encodes a functional secretion signal. A yeast secretion trap assay was performed to test functionality of the predicted signal peptide from FgTPP1 (Zhou et al. 2020). A yeast strain lacking the invertase SUC2 was transformed with pGAD-*FgTPP1*:SUC2$^{22–511}$, which contains a truncated SUC2 gene, without its signal peptide (SUC2$^{22-511}$) fused with full length *FgTPP1*, including its signal peptide sequence, or pGAD-*FgTPP1*$^{\Delta SP}$:SUC2$^{22–511}$, which lacks the predicted signal peptide sequence from *FgTPP1*. As a positive control, the *suc2* yeast mutant was transformed with pGAD-*FgOSP24*:SUC2$^{22–511}$, which contains the full length *FgOSP24* effector from *F. graminearum* and which was previously shown to be secreted from fungal cells (Jiang et al. 2020). The pGAD-*FgTPP1*$^{\Delta SP}$:SUC2$^{22–511}$ and pGAD-SUC2$^{22–511}$ constructs were used as negative controls. Synthetic dropout media (SD) lacking tryptophan and leucine (-TL) supplemented with 2% glucose (Glu) was used as a control media. Images were taken after 4 days of growth and two independent replicates were performed with similar results.

Figure 3. Deletion of the *FgTPP1* gene reduces fungal virulence in bottom inoculated wheat spikes. A, The PH-1-Δ*Fgtpp1-1* mutant did not show an observable virulence defect when wheat spikes were inoculated using the top inoculation method. Yellow arrows indicate inoculation points. Wheat spikes infected either with the Δ*Fgtpp1-1* mutant (PH-1-Δ*Fgtpp1-1*) or wild-type *F. graminearum* PH-1 strain showed similar disease symptoms (left). The number of diseased spikelets throughout the time courses for the Δ*Fgtpp1-1* mutant and wild-type *F. graminearum* PH-1 were similar (middle), and the AUDPC values calculated for the mutant and wild-type did not reveal significant differences (right). Violin plots show distribution of the AUDPC values (black dots), average AUDPC values and confidence intervals (rectangles) for each fungal strain. The statistical analysis (t-test) included pooled data from three independent replicates. Each replicate consisted of 12 plants where 6 plants (one spike per plant) were inoculated either with Δ*Fgtpp1-1* mutant or wild-type *F. graminearum* PH-1 strains (total number of plants inoculated were 17 and 18 for the Δ*Fgtpp1-1* mutant and wild-type *F. graminearum* PH-1 strain, respectively). **B,** The Δ*Fgtpp1* mutants (PH-1-Δ*Fgtpp1-1* and PH-1-Δ*Fgtpp1-3*) show a reduction in virulence with the bottom

inoculation method. The observed number of fully and partially bleached spikes fits to a 1:1 ratio for the wild-type PH-1 strain whilst the observed frequencies for the Δ*Fgtpp1* mutants deviated significantly from the 1:1 ratio ($p < 0.01$). Genetic complementation of the mutant strain Δ*Fgtpp1-1* with a full copy of the *FgTPP1* gene (PH-1-Δ*Fgtpp1-1::TPP1*) restored the virulence defect as the complemented strain fits a 1:1 ratio, which is identical to the wild-type *F. graminearum* PH-1 strain. Each replicate consisted of 60 plants. At the inoculation time, plants at anthesis were selected and a similar number of plants were inoculated with each of the different fungal strains (typically 10 to 14, one spike per plant). Phenotypes were scored at 10 dpi. The statistical analysis included pooled data from four independent replicates. **C,** Representative wheat spike images from the bottom inoculation method at 10 dpi. Yellow arrows indicate inoculation points. Fully bleached spikes consist of bleached and light green spikelets with curved awns along the entire spike. Partially bleached spikes consist of bleached spikelets with curved awns only in the bottom of the spike whilst the upper spikelets remain dark green with straight awns as observed in the mock control. **D**, Partially bleached spikes are consequence of a slow disease progression. Wheat spikes were inoculated either with PH-1-Δ*Fgtpp1-1* mutant or wild-type *F. graminearum* PH-1 strain. Rachises from partially / fully bleached spikes were dissected in 5 segments and plated on plates containing SNA. The presence of the fungus was observed 2 days after plating. Numbers in the bottom right of each picture indicate the number of segments with fungal presence relative to the total number of spike segments evaluated. Three spikes per condition were tested (n=3).

Figure 4. The FgTPP1:GFP fusion protein targets the chloroplast stroma and nucleo-cytosol when transiently expressed in *N. benthamiana*. A, Green Fluorescent Protein (GFP)-tagged FgTPP1 (FgTPP1:GFP) localizes to the chloroplast stroma as well as the nucleo-cytosol in *N. benthamiana* epidermal cells. FgTPP1:GFP or free GFP were transiently co-expressed with mCherry-tagged RbcS-TP (RbcS-TP:mCherry) in *N. benthamiana* leaves using *Agrobacterium*-mediated transformation (agroinfiltration). Images were taken 24 hours post-agroinfiltration (hpi). mCherry-tagged RbcS-TP was included as a reference for chloroplast localization (Helm et al. 2022). All confocal micrographs shown are of single optical sections. The scale bar represents 20 microns. White arrowheads indicate overlapping GFP and mCherry fluorescence signals. **B,** Immunoblot analysis of the FgTPP1:GFP fluorescent protein fusion. The indicated constructs were transiently expressed in *N. benthamiana* leaves. Total protein was isolated 24 hours following agroinfiltration and analyzed using immunoblotting. **C,** mCherry-tagged FgTPP1 localizes to chloroplasts isolated from agroinfiltrated *N. benthamiana*. Leaf tissue transiently expressing FgTPP1:mCherry were harvested 24 hours following agroinfiltration and homogenized in cold isolation buffer. Chloroplasts were isolated as described in the Materials and Methods and imaged using laser-scanning confocal microscopy. Chlorophyll autofluorescence (in blue) was used as a marker for chloroplasts. White arrowheads indicate overlapping mCherry and chlorophyll fluorescence signals. Confocal micrographs from two independent biological replicates are shown in the top and bottom panels. The scale bar shown represents 10 microns.

Figure 5. FgTPP1 suppresses cell surface-trigged and intracellular-mediated immune responses. A, MAPK3 and MAPK6 phosphorylation is induced upon chitin treatment. *N. benthamiana* leaves transiently expressing free GFP (to control for the presence of *A. tumefaciens*) were agroinfiltrated using a needless syringe. Forty-eight hours following agroinfiltration, leaves were infiltrated with chitin (5 µg/mL chitin [hexamer]) and leaf discs (10 mm diameter) harvested at the indicated time points for protein extraction. Anti-phospho-P42/44 antibodies were used to detect phosphorylated MAPK3 and MAPK6. Mock treated leaves were infiltrated with deionized water. Ponceau S staining was used as a loading control. **B,** Chitin-induced accumulation of phosphorylated MAPK3/6 is attenuated by FgTPP1. The indicated constructs were transiently expressed in *N. benthamiana.* Forty-eight hours after agroinfiltration, leaves were infiltrated with chitin (5 µg/mL chitin [hexamer]), total protein extracted at the indicated time points, and immunoblotted using the indicated antibodies. *N. benthamiana* actin and Ponceau S staining were used as loading controls. **C,** Transient expression of FgTPP1:GFP attenuates chitin-induced ROS burst in *N. benthamiana*. FgTPP1:GFP or free GFP were transiently expressed in *N. benthamiana*. Forty-eight hours after agroinfiltration, *N. benthamiana* leaf discs (5 mm diameter) were collected, treated with chitin (5 µg/mL chitin [hexamer]), and relative luminescence (RLU) was monitored for 40 minutes using a previously optimized luminol-based assay (Rogers et al. 2024). **D,** Suppression of $RPS5^{D266E}$-mediated cell death by FgTPP1 in the *N. benthamiana* leaves. *N. benthamiana* leaves were co-infiltrated with *A. tumefaciens* strains carrying myc-tagged $RPS5^{D266E}$ (OD_{600} = 0.15), FgTPP1:sYFP (OD_{600} = 0.3), or empty vector (e.v.; OD_{600} = 0.3). Forty-eight hours following agroinfiltration, *N. benthamiana* leaves were sprayed with 50 µM dexamethasone to induce protein expression. *N. benthamiana* leaves were assessed for cell death and photographed under white and ultraviolet (UV) light 16 hours post-transgene induction. Fractions indicate the number of leaves with observable HR-like cell death / the total number of leaves agroinfiltrated. Experiments were performed three independent times with similar results.

Figure 6. *TPP1* alleles and TPP1 protein haplotypes in *F. graminearum* isolates collected globally. A, Allele networks for the *FgTPP1* coding sequences from 28 *F. graminearum* isolates collected worldwide. Red circles represent one allele and the number within each of the red circles represents the allele number. Each black circle represents the number of mutations between adjacent alleles. The mutated bases in alleles 2 to 7 are compared to allele 1. Five alleles (alleles 1 to 5) encode the protein haplotype isoleucine (I) whilst two alleles (alleles 6 and 7) encode protein haplotype phenylalanine (F). Haplotype networks were generated in POPart using a minimum spanning network. The country of origin and year where each isolate was collected are given between brackets. ARG, Argentina; AUS, Australia; BEL, Belgium, BRA, Brazil; CAN, Canada; FRA, France; DEU, Germany; ITA, Italy; IRN, Iran; LUX, Luxemburg; NDL, Netherlands; POL, Poland; RUS, Russia; USA, United States and ZAF, South Africa. **B**, Amino acid alignment of FgTPP1 for both protein haplotypes. The blue and brown squares represent predicted active sites and binding sites, respectively, between haplotype I and F. Annotations in gray, light violet, and orange lines represent the

predicted signal peptide sequence (SP), the predicted trypsin domain, and the predicted chloroplast targeting signal, respectively. Isoleucine-4 (haplotype I) and phenylalanine-4 (haplotype F) indicate the difference between the two protein haplotypes. Functional secreted signals were predicted for both haplotypes using SignalP v6.0 (Teufel et al. 2022).

Figure 7. Phylogenetic tree of TPP1 protein homologs present in *Fusarium* species and other Ascomycete fungi. *Aspergillus pseudocaelatus* was used as an outgroup. Branches with asterisk (*) are supported by bootstrap value and/or posterior probability with minimum score 70/0.7. Multiple paralogs of TPP1 were present in single isolate of *Alternaria panax*[1], *A. alternata*[2], *A. burnsii*[3], *A. rosae*[4], *F. sarcochroum*[5], *F. torreyae*[6], *F. avenaceum*[7], and *F. tricinctum*[8].

SUPPLEMENTARY FIGURE and TABLE LEGENDS

Supplementary Figure S1. *In vitro* stress tests and DON quantification for wild-type *F. graminearum* PH-1 strain, the *ΔFgtpp1* mutant strains (PH-1-*ΔFgtpp1-1* and PH-1-*ΔFgtpp1-3*, and the complementation strain (PH-1-*ΔFgtpp1-1*::*TPP1*). A, The wild-type *F. graminearum* PH-1 strain was transformed with two PCR fragments containing overlapping sequences of the Hygromycin cassette. Selection of positive transformants was done by multiple PCR amplifications using various primer combinations.t Two independent fungal strains were selected in which the *FgTPP1* gene had been successfully deleted. PCR 1 (primer combination P20 and P21) evaluated the *FgTPP1* coding sequence deletion. PCR2 (primer combination P16 and P17) and PCR3 (primer combination P18 and P19) confirmed correct insertion of the Hygromycin cassette into the *FgTPP1* locus. **B,** Stress tests for wild-type *F. graminearum* PH-1 strain, both *ΔFgtpp1* mutants, and the *ΔFgtpp1* complementation strain. The mutant and the complementation strains showed growth rates and morphology indistinguishable from that of the wild-type *F. graminearum* PH-1 strain for all the conditions evaluated. Images were taken 2 days post-plating on plates. PDA, Potato dextrose agar; SNA, Synthetic nutrient agar; Membrane stresses: Congo Red, Calcofluor, and Tergitol; and salt stress (NaCl). The experiment was repeated twice **C**, No obvious defects were observed in perithecia induction and formation between the PH-1-*ΔFgtpp1-1* mutant and the wild-type *F. graminearum* PH-1 strain. Perithecia images were taken 9 days after perithecia induction on carrot agar medium. **D**, No statistically significant differences in DON mycotoxin production were observed between the *ΔFgtpp1* mutants and wild-type PH-1 strain. DON quantification was performed using wheat spikes infected with either PH-1-*ΔFgtpp1-1,* PH-1-*ΔFgtpp1-3* mutants or the wild-type PH-1 strain. The experiment was repeated twice. Each replicate consisted of 12 plants where three spikes, one spike per plant, were inoculated with the different fungal strains. Mock inoculated spikes were used as negative control. Mock values were reported as < 0.2 ppm as values were outside the lowest calibrator from the standard curve. Data represent the mean of two replicates and error bars denote the 95 % confidence interval (ANOVA followed by Tukey post-hoc test, p value < 0.05). **E**, Diagnostic PCR for the Δ*Fgtpp1* complementation strain (PH-1-ΔFg*tpp1-1*::*TPP1)*. Complementation of the Δ*Fgtpp1-1* mutant strain was done by integration of a cassette containing a wild-type copy of the *FgTPP1* gene including its promoter and terminator into the TSI locus 1. The locus located on chromosome 1 was previously shown to be a haven for complementation analysis. A PCR was performed using primer combination P28 - P29 to evaluate correct insertion of the TPP1 expression cassette containing the TPP1 coding sequence and its native promoter and terminator in the TSI locus 1. PH-1 and the *ΔFgtpp1* mutant strains showed a 2100 base pair amplicon whilst the complementation strain showed an amplicon of 6123 base pair, which indicated insertion of the TPP1 cassette in the TSI locus 1.

Supplementary Figure S2. Representative images of infected wheat spikes using the bottom inoculation method photographed 10 days post-infection. Images belong to a single replicate where wild-type *F. graminearum* PH-1, the *ΔFgtpp1* mutant

strains (PH-1-*ΔFgtpp1-1* and PH-1-*ΔFgtpp1-3*), and the complementation strain (PH-1-*ΔFgtpp1-1*::*TPP1*) were evaluated.

Supplementary Table S1. Accession numbers for the different *F. graminearum* strains included in the FgTPP1 nucleotide and protein haplotype analyses.

Supplementary Table S2. FgTPP1 protein homologs in the *Fusarium* genus.

Supplementary Table S3. Estimates of evolutionary divergence between 28 TPP1 sequences (dN/dS).

Supplementary Table S4. FgTPP1 protein homologs in different genera of the *Ascomycota* phylum.

Supplementary Table S5. List of primers used in this work.

LITERATURE CITED

Ade, J, DeYoung, B, Golstein, C, and Innes, R. 2007. Indirect activation of a plant nucleotide binding site-leucine rich repeat protein by a bacterial protease. Proc Natl Acad Sci USA 104: 2531-2536.

Armer, V.J., Kroll, E., Darino, M., Smith, D., Urban, M., and Hammond-Kosack, K.E. 2024a. Navigating the *Fusarium* species complex: Host-range plasticity and genome variations. Fungal Biol.128: 2439-2459.

Armer, V.J., Urban, M., Ashfield, T., Deeks, M.J. and Hammond-Kosack, K.E. 2024b. The trichothecene mycotoxin deoxynivalenol facilitates cell-to-cell invasion during wheat-tissue colonization by *Fusarium graminearum*. Mol. Plant Pathol. 25: e13485.

Bai, G., and Shaner, G. 2004. Management and resistance in wheat and barley to fusarium head blight. Annu. Rev. Phytopathol. 42: 135-161.

Bentham, A., De la Concepcion, J., Mukhi, N., Zdrzalek, R., Draeger, M., Gorenkin, D., Hughes, R., and Banfield, M. 2020. A molecular roadmap to the plant immune system. J Biol Chem. 295: 14916-14935.

Brown, N.A., Bass, C., Baldwin, T.K., Chen, H., Massot, F., Carion, P.W., Urban, M., van de Meene, A.M.L., and Hammond-Kosack, K.E.. 2011. Characterisation of the *Fusarium graminearum*-wheat floral interaction. J. Pathog. 2011: 626345.

Brown, N.A., Antoniw, J., and Hammond-Kosack, K.E. 2012. The predicted secretome of the plant pathogenic fungus *Fusarium graminearum*: a refined comparative analysis. Plos one. 7:p.e33731.

Brown, N., Evans, J., Mead, A., and Hammond-Kosack, K.E. 2017. A spatial temporal analysis of the *Fusarium graminearum* transcriptome during symptomless and symptomatic wheat infection. Mol. Plant Pathol. 18: 1295-1312.

Camacho, C., Coulouris, G., Avagyan, V., Ma, N., Papadopoulos, J., Bealer, K., and Madden, T.L. 2009. BLAST+: architecture and applications. *BMC Bioinformatics*. 10: 421. https://doi.org/10.1186/1471-2105-10-421.

Carter, M.E., Helm, M., Chapman, A.V.E., Wan, E., Restrepo-Sierra, A.M., Innes, R.W., Bogdanove, A.J., and Wise, R.P. 2019. Convergent evolution of effector protease recognition by *Arabidopsis* and barley. Mol Plant-Microbe Interact. 32: 550-565.

Catlett, N.L., Lee, B-N., Yoder, O., and Turgeon, B.G. 2003. Split-marker recombination for efficient targeted deletion of fungal genes. Fungal Genet. Rep. 50: 9-11.

Cavinder, B., Sikhakolli, U., Fellows, K.M., and Trail, F. 2012. Sexual development and ascospore discharge in *Fusarium graminearum*. J. Vis. Exp. JoVE. 3895: doi:10.3791/3895.

Chandrasekaran, M., Thangavelu, B., Chun, SC., and Sathiyabama, M. 2016. Proteases from phytopathogenic fungi and their importance in phytopathogenicity. J. Gen. Plant Pathol. 82: 233-239.

Chen, J., Zhang, X., Rathjen, J.P., and Dodds, P.N. 2022. Direct recognition of pathogen effectors by plant NLR immune receptors and downstream signaling. Essays Biochem 66: 471-483.

Cuzick, A., Urban, M., and Hammond-Kosack, K. 2008. *Fusarium graminearum* gene deletion mutants *map1* and *tri5* reveal similarities and differences in the pathogenicity requirements to cause disease on Arabidopsis and wheat floral tissue. New Phytol. 177: 990-1000.

Cuomo, C.A., Güldener, U., Xu, J-R., Trail, F., Turgeon, B.G., Di Pietro, A., Walton, J., Ma, L-J., Baker, S., Rep, M., Adam, G., Antoniw, J., Baldwin, T., Calvo, S.,

Chang, Y-L., Decaprio, D., Gale, L., Gnerre, S., Goswami, R., Hammond-Kosack, K., Harris, L., Hilburn, K., Kennell, J., Kroken, S., Magnuson, J., Mannhaupt, G., Mauceli, E., Mewes, H-W., Mitterbauer, R., Muehlbauer, G., Munsterkotter, M., Nelson, D., O'donnell, K., Ouellet, T., Qi, W., Quesneville, H., Roncero, M., Seong, K-Y., Tetko, I., Urban, M., Waalwijk, C., Ward, T., Yao, J., Birren, B., and Kistler, H. 2007. The *Fusarium graminearum* genome reveals a link between localized polymorphism and pathogen specialization. Science. 317:1400–1402.

Darino, M., Urban, M., Kaur, N., Wood, A.M., Grimwade-Mann, M., Smith, D., Beacham, A., and Hammond-Kosack, K.E. 2024. Identification and functional characterisation of a locus for target site integration in *Fusarium graminearum*. Fungal Biol. Biotechnol. 11: doi.org/10.1186/s40694-024-00171-8.

Darma, R., Yu, D.S., Outram, M.A., Sung,Y.-C., Hill, E.H., Croll, D., Williams, S.J., Ovenden, B., Milgate, A., Solomon, P.S., McDonald, M.C. 2024. Revisiting the evolution and function of NIP2 paralogs in the *Rhynchosporium* spp. complex. bioRxiv doi: 10.1101/2024.10.15.618441.

Dean, R., van Kan, J., Pretorius, Z., Hammond-Kosack, K., di Pietro, A., Spanu, P., Rudd, J., Dickman, M., Kahmann, R., Ellis, J., and Foster, G. 2012. The top 10 fungal pathogens in molecular plant pathology. Mol Plant Pathol. 13: 414-430.

Deng, C., Leonard, A., Cahill, J., Lv, M., Li, Y., Thatcher, S., Li, X., Zhao, X., Du, W., Li, Z., Li, H., Llaca, V., Fengler, K., Marshall, L., Harris, C., Tabor, G., Li, Z., Tian, Z., Yang, Q., Chen, Y., Tang, J., Wang, X., Hao, J., Yan, J., Lai, Z., Fei, X., Song, W., Lai, J., Zhang, X., Shu, G., Wang, Y., Chang, Y., Zhu, W., Xiong, W., Sun, J., Li, B., and Ding, J. 2022. The RppC-AvrRppC NLR-effector interaction mediates the resistance to southern corn rust in maize. Mol Plant 15: 904-912.

Ding, P., and Ding, Y. 2020. Stories of salicylic acid: a plant defense hormone. Trends Plant Sci. 25: 549–565.

Engler, C., Gruetzner, R., Kandzia, R., and Marillonnet, S. 2009. Golden gate shuffling: a one-pot DNA shuffling method based on type IIs restriction enzymes. PLoS ONE. 4: e5553.

Figueroa, M., Hammond-Kosack, K.E, and Solomon, P. 2018. A review of wheat diseases–a field perspective. Mol Plant Pathol. 19: 1523-1536.

Figueroa, M., Ortiz, D., and Henningsen, E.C. 2021. Tactics of host manipulation by intracellular effectors from plant pathogenic fungi. Curr. Opin. Plant Biol. 62: 102054.

Galvez-Valdivieso, G., and Mullineaux, P.M. 2010. The role of reactive oxygen species in signaling from chloroplasts to the nucleus. Physiol. Planta 138: 430-439.

Hao, G., McCormick, S., Vaughan, M., Naumann, T., Kim, H-S., Proctor, R. Kelly, A., and Ward, T. 2019. *Fusarium graminearum* arabinanase (Arb93B) enhances wheat head blight susceptibility by suppressing plant immunity. Mol Plant Microbe Interact. 32: 888-898.

Hao, G., McCormick, S., Usgaard, T., Tiley, H., and Vaughan, M. 2020. Characterization of three *Fusarium graminearum* effectors and their roles during Fusarium Head Blight. Front. Plant Sci. 11: 579553.

Hao, G., Nauman, T., Chen, H., Bai, G., McCormick, S., Kim, H-S., Tian, B., Trick, H., Naldrett, M., and Proctor, R. 2023. *Fusarium graminearum* effector FgNls1 targets plant nuclei to induce wheat head blight. Mol Plant-Microbe Interact. 36: 478-488.

Helm, M., Qi, M., Sarkar, S., Yu, H., Whitham, SA., and Innes, RW. 2019. Engineering a decoy substrate in soybean to enable recognition of the *Soybean Mosaic Virus* NIa protease. Mol Plant-Microbe Interact. 32: 760-769.

Helm, M., Singh, R., Hiles, R., Jaiswal, N., Myers, A., Iyer-Pascuzzi, A. S., and Goodwin, B. S. 2022. Candidate effector proteins from the maize tar spot pathogen *Phyllachora maydis* localize to diverse plant cell compartments. Phytopathology. 112: 2538–2548.

Hohn, T.M., and Desjardins, A.E. 1992. Isolation and gene disruption of the *Tox5* gene encoding trichodiene synthase in *Gibberella pulicaris*. Mol. Plant Microbe Interact. 5: 249-56.

Huelsenbeck, J.P., and Ronquist, F. 2001. MRBAYES: Bayesian inference of phylogenetic trees. Bioinformatics. 17: 754-755.

Jaiswal, N., Liao, C-J., Mengesha, B., Han, H., Lee, S., Sharon, A., Zhou, Y., and Mengiste, T. 2022. Regulation of plant immunity and growth by tomato receptor-like cytoplasmic kinase TRK1. New Phytol. 233: 458-478.

Jaiswal, N., Myers, A., Weese, T.L., Carter, M.E., Scofield, S.R., and Helm, M. 2023. Analysis of cell death induction by the barley NLR immune receptor PBR1. PhytoFrontiers. 3: 663-678.

Jashni, MK., Mehrabi, R., Collemare, J., Mesarich, CH., and de Wit PJGM. 2015. The battle in the apoplast: further insights into the roles of proteases and their inhibitors in plant-pathogen interactions. Front Plant Sci. 6: 584.

Jiang, C., Hei, R., Yang, Y., Zhang, S., Wang, Q., Wang, W., Zhang, Q., Yan, M., Zhu, G., Huang, P., Liu, H., and Xu, J-R. 2020. An orphan protein of *Fusarium graminearum* modulates host immunity by mediating proteasomal degradation of TaSnRK1α. Nat Commun. 11: 4382.

Johns, L.E., Bebber, D.P., Gurr, S.J., and Brown, N.A. 2022. Emerging health threat and cost of Fusarium mycotoxins in European wheat. Nature Food. 3: 1014-1019.

Kalyaanamoorthy, S., Minh, B.Q., Wong, T.K.F., von Haeseler, A., and Jermiin, L.S. 2017. ModelFinder: fast model selection for accurate phylogenetic estimates. Nat. Methods. 14: 587-589.

Kanja, C., Machado-Wood, A., Baggaley, L., Walker, C., and Hammond-Kosack, K.E. 2021. Cereal-Fusarium interactions: improved fundamental insights into Fusarium pathogenomics and cereal host resistance reveals new ways to achieve durable disease control. In the book ‘ Achieving durable disease resistance in cereals’, Editor R. Oliver. Burleigh Dodds Science Publishing, 79pp.

Kim, M., Cunha, L., McFall, A., Belkhadir, Y., DebRoy, S., Dangl, J., and Mackey, D. 2005. Two *Pseudomonas syringae* type III effectors inhibit RIN4-regulated basal defense in Arabidopsis. Cell. 121: 749-759.

Kim, S.H., Qi, D., Ashfield, T., Helm, M., and Innes, RW. 2016. Using decoys to expand the recognition specificity of a plant disease resistance protein. Science. 351: 684-687.

King, R., Urban, M., Hammond-Kosack, M.C., Hassani-Pak, K., and Hammond-Kosack, K.E. 2015. The completed genome sequence of the pathogenic ascomycete fungus *Fusarium graminearum*. BMC Genomics. 16: 544.

King, R., Urban, M., and Hammond-Kosack, K.E. 2017a. Annotation of *Fusarium graminearum* (PH-1) Version 5.0. Genome Announc. 5: e01479-16.

King, R., Urban, M., Lauder, R.P., Hawkins, N., Evans, M., Plummer, A., Halsey, K., Lovegrove, A., Hammond-Kosack, K.E., and Rudd, J.J. 2017b. A conserved fungal glycosyltransferase facilitates pathogenesis of plants by enabling hyphal growth on solid surfaces. PLoS pathogens, 13: p.e1006672.

Kretschmer, M., Damoo, D., Djamei, A., and Kronstad, J. 2020. Chloroplasts and plant immunity: where are the fungal effectors? Pathogens 9: 19.

Kroll, E., Bayon, C., Rudd, J.J., Armer, V., Magaji-Umashankar, A., Ames, R., Urban, M., Brown, N.A., Hammond-Kosack, K.E. 2025. A conserved fungal Knr4/Smi1 protein is vital for maintaining cell wall integrity and host plant pathogenesis. PLoS Pathogens *(In press).*

Lampropoulos, A., Sutikovic, Z., Wenzl, C., Maegele, I., Lohmann, J.U. and Forner, J. 2013. GreenGate-a novel, versatile, and efficient cloning system for plant transgenesis. PloS one, 8:p.e83043.

Leigh, J.W., and Bryant, D. 2015. PopART: Full-feature software for haplotype network construction. Methods Ecol. Evol. 6: 1110-1116.

Littlejohn, G.R., Breen, S., Smirnoff, N., and Grant, M. 2021. Chloroplast immunity illuminated. New Phytol. 229: 3088-3107.

Liu, K., Wang, X., Qi, Y., Li, Y., Shi, Y., Ren, Y., Wang, A., Cheng, P., and Wang, B. 2024. Effector protein serine carboxypeptidase FgSCP is essential for full virulence in *F. graminearum* and is involved in modulating plant immune responses. Phytopathology. DOI: 10.1094/PHYTO-02-24-0068-R

Liu, J., Gong, P., Lu, R., Lozano-Duran, R., Zhou, X., Li, F. 2024. Chloroplast immunity: a cornerstone of plant defense. Mol Plant 17: 686-688.

Lu, S., and Edwards, MC. 2016. Genome-wide analysis of small secreted cysteine-rich proteins identifies candidate effector proteins potentially involved in *Fusarium graminearum*-wheat interactions. Phytopathology. 106: 166-76.

McCombe, C.L., Greenwood, J.R., Solomon, P.S., and Williams, S.J. 2022. Molecular plant immunity against biotrophic, hemibiotrophic, and necrotrophic fungi. Essays Biochem 66: 581-593.

Menke, J, R. 2011. A study of *Fusarium graminearum* virulence factors. [Doctoral dissertation, University of Minnesota]. https://hdl.handle.net/11299/119322.

Meng, E.C., Goddard, T.D., Pettersen, E.F., Couch, G.S., Pearson, Z.J., Morris, J.H., and Ferrin, T.E. 2023. UCSF: ChimeraX: Tools for structure building and analysis. Protein Sci. 32: e4792.

Mentges, M., Glasenapp, A., Boenisch, M., Malz, S., Henrissat, B., Frandsen, R., Guldener, U., Munsterkotter, M., Bormann, J., Lebrun, M-H., Schafer, W., and Martinez-Rocha, A. 2020. Infection cushions of *Fusarium graminearum* are fungal arsenals for wheat infection. Mol Plant Pathol. 21: 1070-1087.

Miltenburg, M., Bonner, C., Hepworth, S., Huang, M., Rampitsch, C., and Subramaniam, R. 2022. Proximity-dependent biotinylation identified a suite of candidate effector proteins from *Fusarium graminearum*. Plant J. 112: 369-382.

Mirdita, M., Schutze, K., Moriwaki, Y., Heo, L., Ovchinnikov, S., and Steinegger, M. 2022. ColabFold: making protein folding accessible to all. Nat Methods. 19: 679-682.

Nelson, B.K., Cai, X., and Nebenfuhr, A. 2007. A multicolored set of *in vivo* organelle markers for co-localization studies in Arabidopsis and other plants. Plant J. 51: 1126-1136.

Nganje, WE., Kaitibie, S., Wilson, WW., Leistritz, FL., and Bangsund, DA. 2004. Economic impacts of Fusarium Head Blight in wheat and barley: 1993-2001. Agribusiness and Applied Economics Report No 538. July.

Ngou, B.P.M., Ding, P., and Jones, J.D.G. 2022. Thirty years of resistance: Zig-zag through the plant immune system. Plant Cell 34: 1447-1478.

Nguyen, L.T., Schmidt, H.A., von Haeseler, A., and Minh, B.Q. 2015. IQ-TREE: a fast and effective stochastic algorithm for estimating maximum-likelihood phylogenies. Mol. Biol. Evol. 32: 268-274.

Petre, B., Saunders, D.G.O., Sklenar, J., Lorrain, C., Win, J., Duplessis, S., and Kamoun, S. 2015. Candidate effector proteins of the rust pathogen *Melampsora larici-populina* target diverse plant cell compartments. Mol. Plant Microbe Interact. 28: 689-700.

Petre, B., Lorrain, C., Saunders, D.G.O., Win, J., Sklenar, J., Duplessis, S., and Kamoun, S. 2016. Rust fungal effectors mimic host transit peptides to translocate into chloroplasts. Cell Microbiol. 18: 453-465.

Pottinger, S.E., Bak, A., Margets, A., Helm, M., Tang, L., Casteel, C., and Innes, RW. 2020. Optimizing the PBS1 decoy system to confer resistance to Potyvirus infection in Arabidopsis and soybean. Mol Plant-Microbe Interact. 33: 932-944.

Qi, D., DeYoung, B.J., and Innes, R.W. 2012. Structure-function analysis of the coiled-coil and leucine-rich repeat domains of the *RPS5* disease resistance protein. Plant Physiol. 158: 1819-1832.

Qiu, H., Zhao, X., Fang, W., Wu, H., Abubakar, Y., Lu, G., Wang, Z., and Zheng, W. 2019. Spatiotemporal nature of *Fusarium graminearum*-wheat coleoptile interactions. Phytopathol Res 1: 26.

Rambaut, A. 2018. FigTree v1.4.4: Molecular Evolution, Phylogenetics and Epidemiology. Edinburgh: University of Edinburgh.

Redditt, T., Chung, E-H., Karimi, H., Rodibaugh, N., Zhang, Y., Trinidad, J., Kim, J., Zhou, Q., Shen, M., Dangl, J., Mackey, D., and Innes, R. 2019. AvrRpm1 functions as an ADP-ribosyl transferase to modify NOI domain-containing proteins, including Arabidopsis and soybean RPM1-Interacting Protein 4. Plant Cell. 31: 2664-2681.

Rhodes, J., Zipfel, C., Jones, J.D.G., and Ngou, B.P.M. 2022. Concerted actions of PRR- and NLR-mediated immunity. Essays Biochem 66: 501-511.

Robert-Seilaniantz, A., Grant, M., and Jones, J. D. 2011. Hormone crosstalk in plant disease and defense: more than just jasmonate-salicylate antagonism. Annu. Rev. Phytopathol. 49: 317-343.

Rogers, A., Jaiswal, N., Roggenkamp, E., Kim, H-S., MacCready, J., Chilvers, M., Scofield, S., Iyer-Pascuzzi, A., and Helm, M. 2024. Genome-informed trophic classification and functional characterization of virulence proteins from the maize tar spot pathogen *Phyllachora maydis*. Phytopathology. 114: 1940-1949.

Rudd, J.J., Antoniw, J., Marshall, R., Motteram, J., Fraaije, B., and Hammond-Kosack, K. 2010. Identification and characterisation of *Mycosphaerella graminicola* secreted or surface-associated proteins with variable intragenic coding repeats. Fungal Genet. Biol. 47: 19-32.

Schandry, N. 2017. A practical guide to visualization and statistical analysis of *R. solanacearum* infection data using R. R. Front. Plant Sci. 8:623.

Selin, C., de Kievit, TR., Belmonte, MF., and Fernando WGD. 2016. Elucidating the role of effectors in plant-fungal interactions: progress and challenges. Front Microbiol. 7: 600.

Seong, K., Hou, Z.M., Tracy, M., Kistler, H.C., and Xu, J.R. 2005. Random insertional mutagenesis identifies genes associated with virulence in the wheat scab fungus *Fusarium graminearum*. Phytopathology. 95: 744-750.

Shao, F, Golstein, C, Ade, J, Stoutemyer, M, Dixon, J, and Innes, R. 2003. Cleavage of *Arabidopsis* PBS1 by a bacterial type III effector. Science 301: 1230-1233.

Simonich, M, and Innes, R. 1995. A disease resistance gene in *Arabidopsis* with specificity for the *avrPph3* gene of *Pseudomonas syringae* pv. *phaseolicola*. Mol Plant Microbe Interact 8: 637-640.

Simons, G., Groenendijk, J., Wijbrandi, J., Reijans, M., Groenen, J., Diergaarde, P., Van der Lee, T., Bleeker, M., Onstenk, J., de Both, M., Haring, M., Mes, J., Cornelissen, B., Zabeau, M., and Vos, P. 1998. Dissection of the *Fusarium* I2 gene cluster in tomato reveals six homologs and one active gene copy. Plant Cell 10: 1055-1068.

Sperschneider, J., Catanzariti, A.M., DeBoer, K., Petre, B., Gardiner, D.M., Singh, K.B., Dodds, P.N., and Taylor, J.M. 2017. LOCALIZER: subcellular localization prediction of both plant and effector proteins in the plant cell. Sci. Rep. 7: 44598.

Tamura, K. and Nei, M. 1993. Estimation of the number of nucleotide substitutions in the control region of mitochondrial DNA in humans and chimpanzees. Molecular Biology and Evolution 10: 512-526.

Tamura, K., Stecher, G., and Kumar, S. 2021. MEGA 11: Molecular Evolutionary Genetics Analysis Version 11. Molecular Biology and Evolution https://doi.org/10.1093/molbev/msab120.

Teufel, F., Almagro Armenteros, J.J., Johansen, A.R., Gislason, M.H., Pihl, S.I., Tsirigos, K.D., Winther, O., Brunak, S., von Heijne, G., Nielsen, H. 2022. SignalP 6.0 predicts all five types of signal peptides using protein language models. Nat. Biotechnol. doi.org/10.1038/s41587-021-01156-3.

Trotta, A., Rahikainen, M., Konert, G., Finazzi, G. & Kangasjarvi, S. 2014. Signaling crosstalk in light stress and immune reactions in plants. Phil. Trans. R. Soc. B 369, 20130235.

Urban, M., Mott, E., Farley, T., and Hammond-Kosack, K. 2003. The *Fusarium graminearum MAP1* gene is essential for pathogenicity and development of perithecia. Mol. Plant Pathol. 4: 347–59.

Vinatzer, B.A., Teitzel, G.M., Lee, M.-W., Jelenska, J., Hotton, S., Fairfax, K., Jenrette, J., and Greenberg, J.T. 2006. The type III effector repertoire of *Pseudomonas syringae pv. syringae* B728a and its role in survival and disease on host and non-host plants. Mol. Microbiol. 62: 26-44.

Waalwijk, C., Taga, M., Zheng, S.-L., Proctor, R.H., Vaughan, M.M., and O'Donnell. 2018. Karyotype evolution in *Fusarium*. IMA Fungus 9:13-26.

Wang, C., Zheng, Y., Liu, Z., Qian, Y., Li, Y., Yang, L., Liu, S., Liang, W., and Li, J. 2023. The secreted FolAsp aspartic protease facilitates the virulence of *Fusarium oxysporum* f. sp. *lycopersici*. Front. Microbiol. 14: 1103418.

Wang, X., He, M., Liu, H., Ding, H., Liu, K., Li, y., Cheng, P., Li, Q., and Wang, B. 2022. Functional characterization of the M36 metalloprotease FgFly1 in *Fusarium graminearum*. J. Fungi. 8: 726.

Wood, A.K., Walker, C., Lee, W-S., Urban, M., and Hammond-Kosack, K.E. 2020. Functional evaluation of a homologue of plant rapid alkalinisation factor (RALF) peptides in *Fusarium graminearum*. Fungal Biol. 124: 753-765.

Xiong, J., Luo, M., Chen, Y., Hu, Q., Fang, Y., Sun, T., Hu, G., and Zhang, C-J. 2024. Subtilisin-like proteases from *Fusarium graminearum* induce plant cell death and contribute to virulence. Plant Physiol. 195: 1681-1693.

Xu, L., Wang, H., Zhang, C., Wang, J., Chen, A., Chen, Y., and Ma, Z. 2020. System-wide characterization of subtilases reveals that subtilisin-like protease FgPrb1 of *Fusarium graminearum* regulates fungal development and virulence. Fungal Genet. Biol. 144: 103449.

Xu, Q., Tang, C., Wang, X., Sun, S., Zhao, J., Kang, Z., and Wang, X. 2019. An effector protein of the wheat stripe rust fungus targets chloroplasts and suppresses chloroplast function. Nat. Commun. 10: 5571.

Zhang, J, Li, W, Xiang, T, Liu, Z, Laluk, K, Ding, X, Zou, Y, Gao, M, Zhang, X, Chen, S, Mengiste, T, Zhang, Y, and Zhou, J. 2010. Receptor-like cytoplasmic kinases integrate signaling from multiple plant immune receptors and are targeted by a *Pseudomonas syringae* effector. Cell Host Microbe 7: 290-301.

Zhou, B., Benbow, H.R., Brennan, C.J., Arunachalam, C., Karki, S.J., Mullins, E., Feechan, A., Burke, J.I., and Doohan, F.M. 2020. Wheat encodes small, secreted proteins that contribute to resistance to Septoria tritici blotch. Front. Genet. 11: 469.

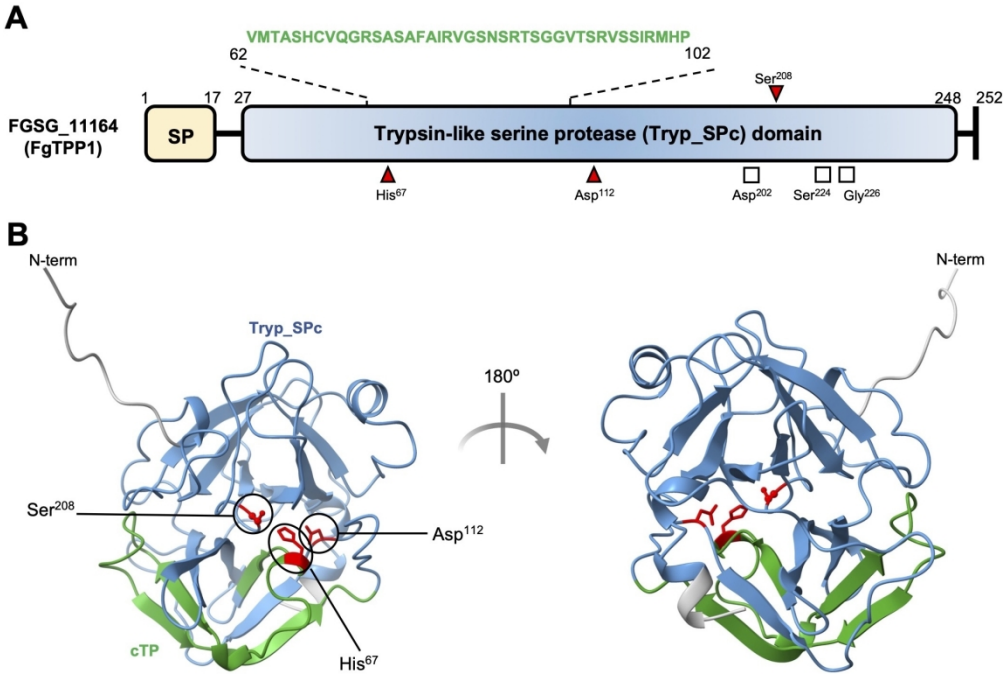

Figure 1. Schematic illustration and predicted protein structure of FgTPP1 (FGSG_11164). A, Schematic representation of the F. graminearum candidate effector protease FgTPP1 including the putative signal peptide (SP; aa 1-17) sequence and the predicted trypsin-like serine protease (Tryp_SPc; aa 27-248) domain. The predicted chloroplast targeting motif (aa 62-102) is indicated in green. Putative catalytic active sites (His-67, Asp-112, and Ser-208) are indicated by red triangles and predicted substrate binding sites (Asp-202, Ser-224, and Gly-226) are indicated by white squares. Numbers delineate amino acid positions. B, The predicted three-dimensional protein structure of FgTPP1 as determined by AlphaFold2. The predicted trypsin-like serine protease domain is indicated in light blue, the chloroplast targeting motif is indicated in green, and the putative catalytic residues are indicated in red. N-term: amino terminus.

740x502mm (72 x 72 DPI)

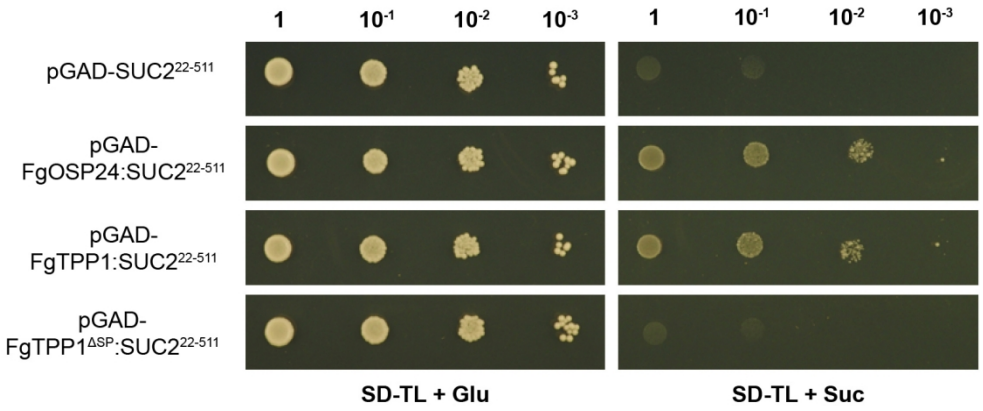

Figure 2. The FgTPP1 protein encodes a functional secretion signal. A yeast secretion trap assay was performed to test functionality of the predicted signal peptide from FgTPP1 (Zhou et al. 2020). A yeast strain lacking the invertase SUC2 was transformed with pGAD-FgTPP1:SUC222–511, which contains a truncated SUC2 gene, without its signal peptide (SUC222-511) fused with full length FgTPP1, including its signal peptide sequence, or pGAD-FgTPP1ΔSP:SUC222–511, which lacks the predicted signal peptide sequence from FgTPP1. As a positive control, the suc2 yeast mutant was transformed with pGAD-FgOSP24:SUC222–511, which contains the full length FgOSP24 effector from F. graminearum and which was previously shown to be secreted from fungal cells (Jiang et al. 2020). The pGAD-FgTPP1ΔSP:SUC222–511 and pGAD-SUC222–511 constructs were used as negative controls. Synthetic dropout media (SD) lacking tryptophan and leucine (-TL) supplemented with 2% glucose (Glu) was used as a control media. Images were taken after 4 days of growth and two independent replicates were performed with similar results.

141x59mm (300 x 300 DPI)

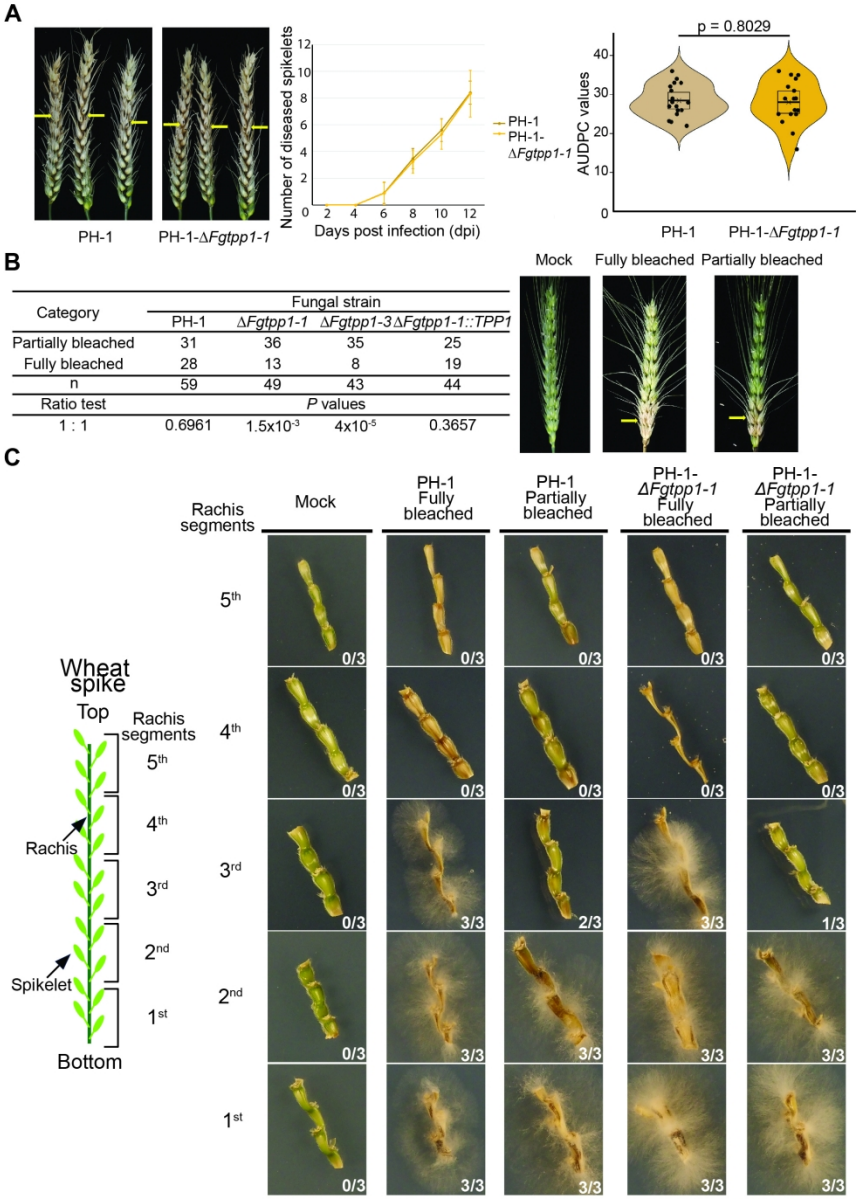

Category	Fungal strain			
	PH-1	*ΔFgtpp1-1*	*ΔFgtpp1-3*	*ΔFgtpp1-1::TPP1*
Partially bleached	31	36	35	25
Fully bleached	28	13	8	19
n	59	49	43	44
Ratio test	*P* values			
1 : 1	0.6961	$1.5x10^{-3}$	$4x10^{-5}$	0.3657

Figure 3. Deletion of the FgTPP1 gene reduces fungal virulence in bottom inoculated wheat spikes. A, The PH-1-ΔFgtpp1-1 mutant did not show an observable virulence defect when wheat spikes were inoculated using the top inoculation method. Yellow arrows indicate inoculation points. Wheat spikes infected either with the ΔFgtpp1-1 mutant (PH-1-ΔFgtpp1-1) or wild-type F. graminearum PH-1 strain showed similar disease symptoms (left). The number of diseased spikelets throughout the time courses for the ΔFgtpp1-1 mutant and wild-type F. graminearum PH-1 were similar (middle), and the AUDPC values calculated for the mutant and wild-type did not reveal significant differences (right). Violin plots show distribution of the AUDPC values (black dots), average AUDPC values and confidence intervals (rectangles) for each fungal strain. The statistical analysis (t-test) included pooled data from three independent replicates. Each replicate consisted of 12 plants where 6 plants (one spike per plant) were inoculated either with ΔFgtpp1-1 mutant or wild-type F. graminearum PH-1 strains. B, The ΔFgtpp1 mutants (PH-1-ΔFgtpp1-1 and PH-1-ΔFgtpp1-3) show a reduction in virulence with the bottom inoculation method. The observed number of fully and partially bleached spikes fits to a 1:1 ratio for the wild-type PH-1 strain whilst the observed frequencies for

the ΔFgtpp1 mutants deviated significantly from the 1:1 ratio ($p < 0.01$). Genetic complementation of the mutant strain ΔFgtpp1-1 with a full copy of the FgTPP1 gene (PH-1-ΔFgtpp1-1::TPP1) restored the virulence defect. Phenotypes were scored at 10 dpi. The statistical analysis included pooled data from four independent replicates. C, Representative wheat spike images from the bottom inoculation method at 10 dpi. Yellow arrows indicate inoculation points. Fully bleached spikes consist of bleached and light green spikelets with curved awns along the entire spike. Partially bleached spikes consist of bleached spikelets with curved awns only in the bottom of the spike whilst the upper spikelets remain dark green with straight awns as observed in the mock control. D, Partially bleached spikes are consequence of a slow disease progression. Wheat spikes were inoculated either with PH-1-ΔFgtpp1-1 mutant or wild-type F. graminearum PH-1 strain. Rachises from partially / fully bleached spikes were dissected in 5 segments and plated on plates containing SNA. The presence of the fungus was observed 2 days after plating. Numbers in the bottom right of each picture indicate the number of segments with fungal presence relative to the total number of spike segments evaluated. Three spikes per condition were tested (n=3).

177x246mm (300 x 300 DPI)

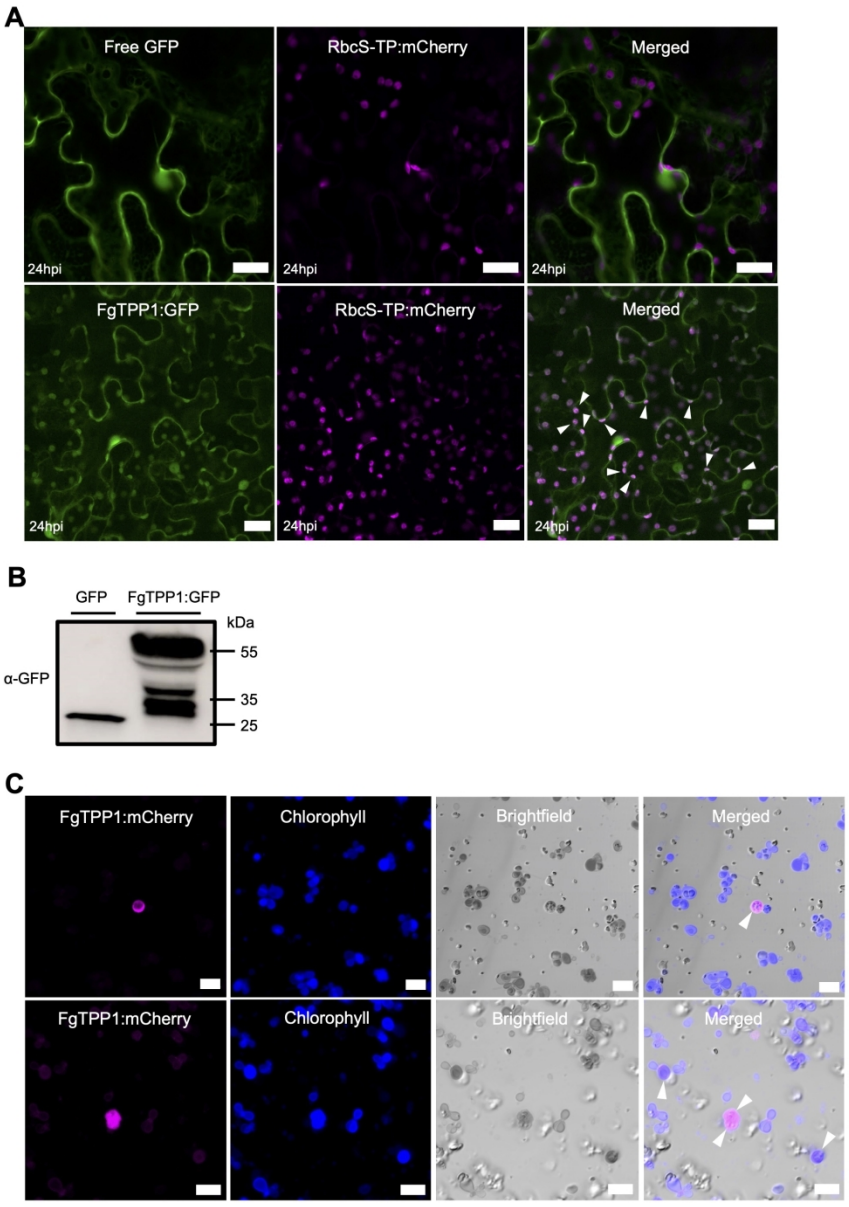

Figure 4. The FgTPP1:GFP fusion protein targets the chloroplast stroma and nucleo-cytosol when transiently expressed in N. benthamiana. A, Green Fluorescent Protein (GFP)-tagged FgTPP1 (FgTPP1:GFP) localizes to the chloroplast stroma as well as the nucleo-cytosol in N. benthamiana epidermal cells. FgTPP1:GFP or free GFP were transiently co-expressed with mCherry-tagged RbcS-TP (RbcS-TP:mCherry) in N. benthamiana leaves using Agrobacterium-mediated transformation (agroinfiltration). Images were taken 24 hours post-agroinfiltration (hpi). mCherry-tagged RbcS-TP was included as a reference for chloroplast localization (Helm et al. 2022). All confocal micrographs shown are of single optical sections. The scale bar represents 20 microns. White arrowheads indicate overlapping GFP and mCherry fluorescence signals. B, Immunoblot analysis of the FgTPP1:GFP fluorescent protein fusion. The indicated constructs were transiently expressed in N. benthamiana leaves. Total protein was isolated 24 hours following agroinfiltration and analyzed using immunoblotting. C, mCherry-tagged FgTPP1 localizes to chloroplasts isolated from agroinfiltrated N. benthamiana. Leaf tissue transiently expressing FgTPP1:mCherry were harvested 24 hours following agroinfiltration and homogenized in cold isolation buffer. Chloroplasts were isolated as described in the Materials and Methods and imaged using laser-scanning confocal microscopy. Chlorophyll autofluorescence

(in blue) was used as a marker for chloroplasts. White arrowheads indicate overlapping mCherry and chlorophyll fluorescence signals. Confocal micrographs from two independent biological replicates are shown in the top and bottom panels. The scale bar shown represents 10 microns.

740x1025mm (72 x 72 DPI)

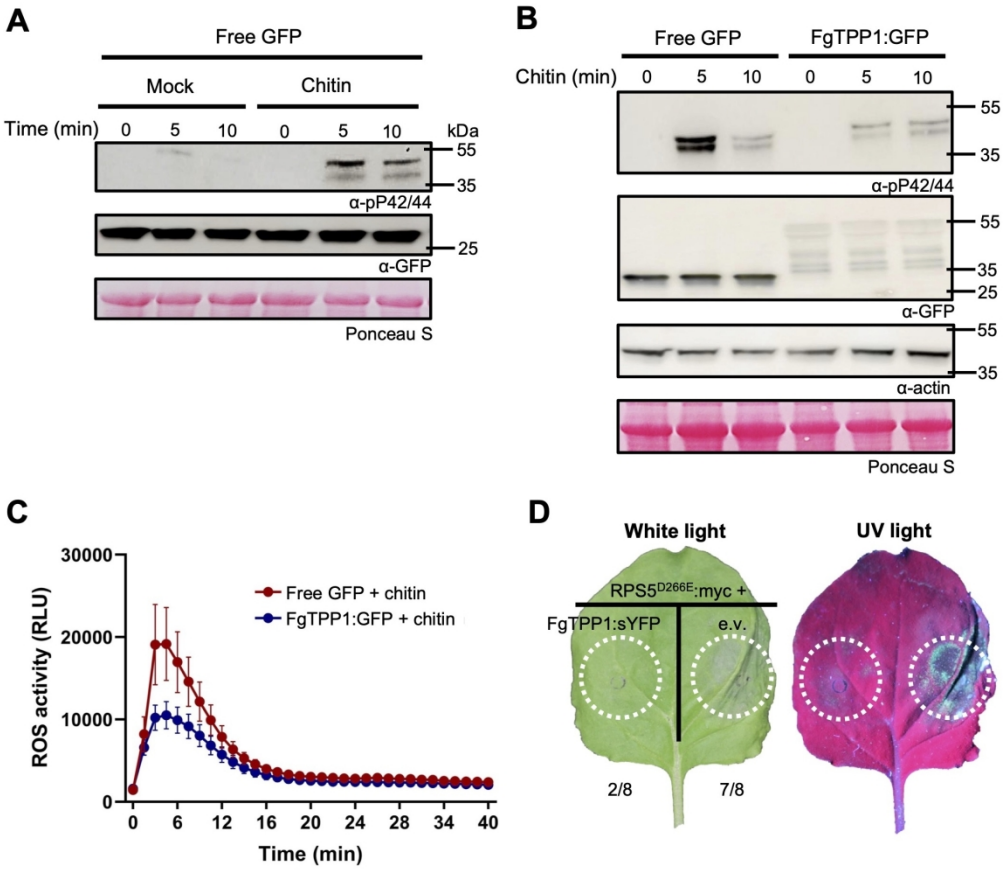

Figure 5. FgTPP1 suppresses cell surface-trigged and intracellular-mediated immune responses. A, MAPK3 and MAPK6 phosphorylation is induced upon chitin treatment. N. benthamiana leaves transiently expressing free GFP (to control for the presence of A. tumefaciens) were agroinfiltrated using a needless syringe. Forty-eight hours following agroinfiltration, leaves were infiltrated with chitin (5 µg/mL chitin [hexamer]) and leaf discs (10 mm diameter) harvested at the indicated time points for protein extraction. Anti-phospho-P42/44 antibodies were used to detect phosphorylated MAPK3 and MAPK6. Mock treated leaves were infiltrated with deionized water. Ponceau S staining was used as a loading control. B, Chitin-induced accumulation of phosphorylated MAPK3/6 is attenuated by FgTPP1. The indicated constructs were transiently expressed in N. benthamiana. Forty-eight hours after agroinfiltration, leaves were infiltrated with chitin (5 µg/mL chitin [hexamer]), total protein extracted at the indicated time points, and immunoblotted using the indicated antibodies. N. benthamiana actin and Ponceau S staining were used as loading controls. C, Transient expression of FgTPP1:GFP attenuates chitin-induced ROS burst in N. benthamiana. FgTPP1:GFP or free GFP were transiently expressed in N. benthamiana. Forty-eight hours after agroinfiltration, N. benthamiana leaf discs (5 mm diameter) were collected, treated with chitin (5 µg/mL chitin [hexamer]), and relative luminescence (RLU) was monitored for 40 minutes using a previously optimized luminol-based assay (Rogers et al. 2024). D, Suppression of RPS5D266E-mediated cell death by FgTPP1 in the N. benthamiana leaves. N. benthamiana leaves were co-infiltrated with A. tumefaciens strains carrying myc-tagged RPS5D266E (OD600 = 0.15), FgTPP1:sYFP (OD600 = 0.3), or empty vector (e.v.; OD600 = 0.3). Forty-eight hours following agroinfiltration, N. benthamiana leaves were sprayed with 50 µM dexamethasone to induce protein expression. N. benthamiana leaves were assessed for cell death and photographed under white and ultraviolet (UV) light 16 hours post-transgene induction. Fractions indicate the number of leaves with observable HR-like cell death / the total number of leaves agroinfiltrated. Experiments were performed three independent times with similar results.

740x644mm (72 x 72 DPI)

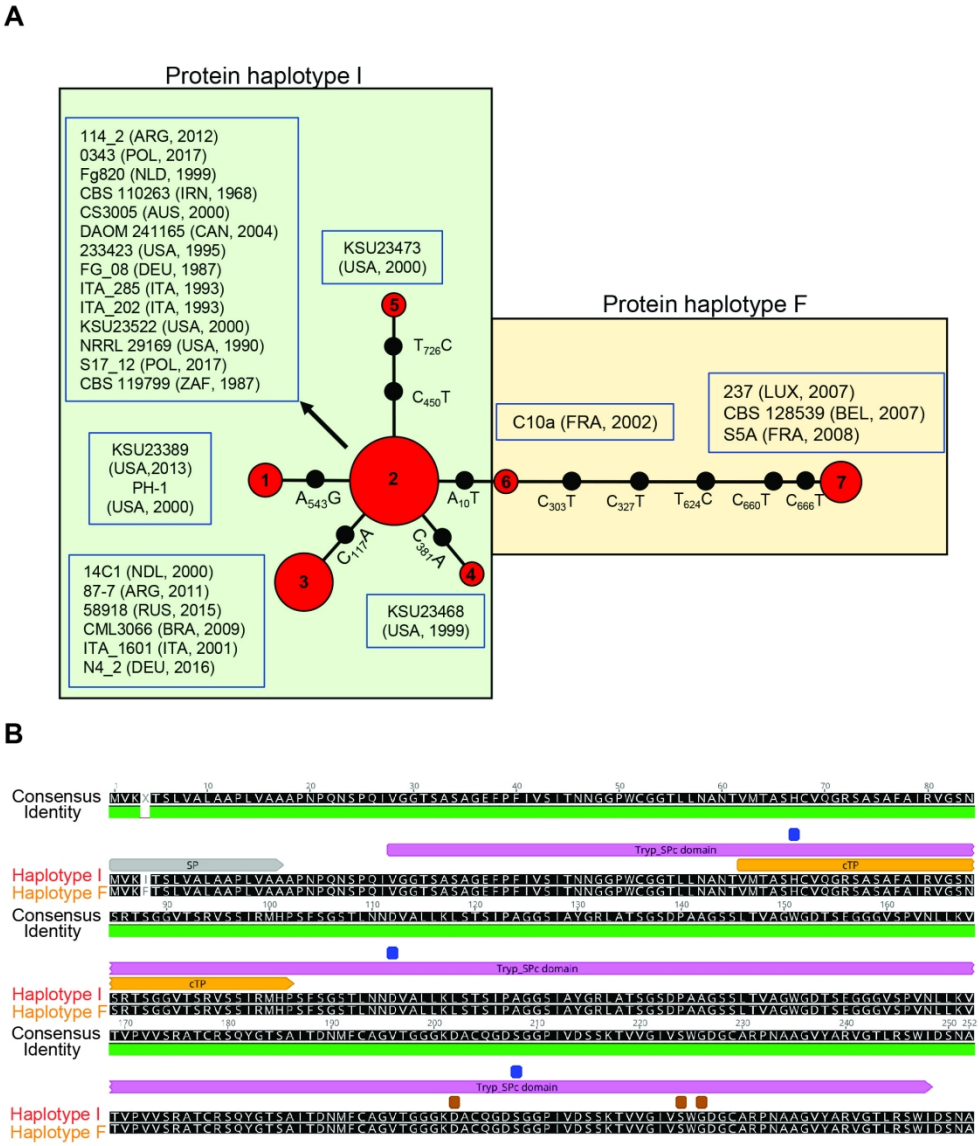

Figure 6. TPP1 alleles and TPP1 protein haplotypes in F. graminearum isolates collected globally. A, Allele networks for the FgTPP1 coding sequences from 28 F. graminearum isolates collected worldwide. Red circles represent one allele and the number within each of the red circles represents the allele number. Each black circle represents the number of mutations between adjacent alleles. The mutated bases in alleles 2 to 7 are compared to allele 1. Five alleles (alleles 1 to 5) encode the protein haplotype isoleucine (I) whilst two alleles (alleles 6 and 7) encode protein haplotype phenylalanine (F). Haplotype networks were generated in POPart using a minimum spanning network. The country of origin and year where each isolate was collected are given between brackets. ARG, Argentina; AUS, Australia; BEL, Belgium, BRA, Brazil; CAN, Canada; FRA, France; DEU, Germany; ITA, Italy; IRN, Iran; LUX, Luxemburg; NDL, Netherlands; POL, Poland; RUS, Russia; USA, United States and ZAF, South Africa. B, Amino acid alignment of FgTPP1 for both protein haplotypes. The blue and brown squares represent predicted active sites and binding sites, respectively, between haplotype I and F. Annotations in gray, light violet, and orange lines represent the predicted signal peptide sequence (SP), the predicted trypsin domain, and the predicted chloroplast targeting signal, respectively. Isoleucine-4 (haplotype I) and phenylalanine-4 (haplotype F) indicate the difference between the two protein haplotypes. Functional secreted signals were predicted for both haplotypes using SignalP

v6.0 (Teufel et al. 2022).

177x208mm (300 x 300 DPI)

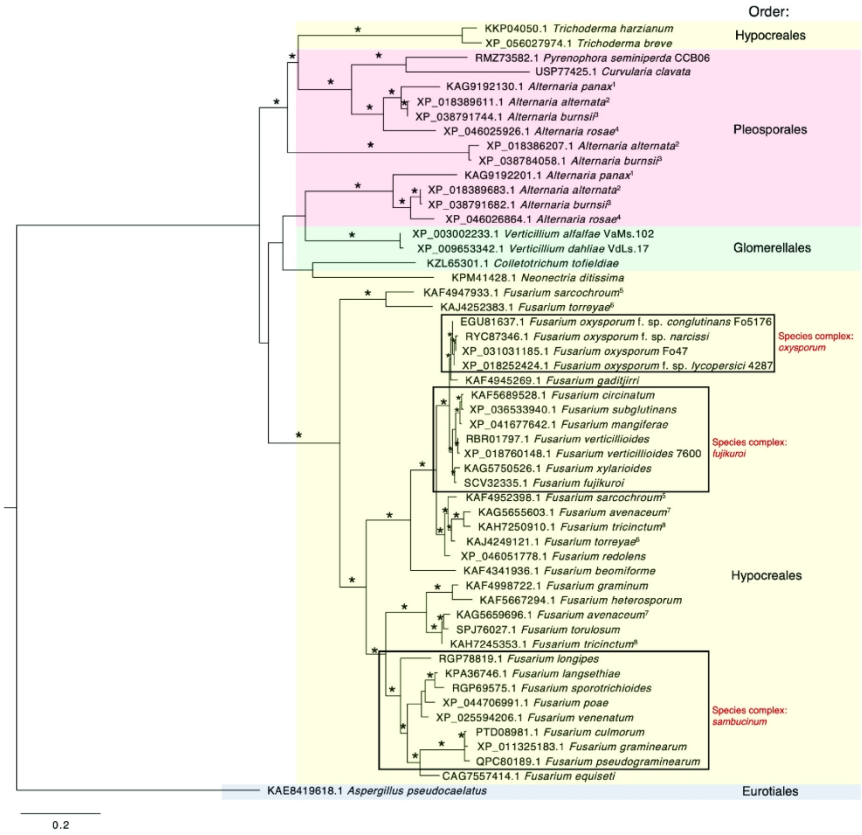

Figure 7. Phylogenetic tree of TPP1 protein homologs present in Fusarium species and other Ascomycete fungi. Aspergillus pseudocaelatus was used as an outgroup. Branches with asterisk (*) are supported by bootstrap value and/or posterior probability with minimum score 70/0.7. Multiple paralogs of TPP1 were present in single isolate of Alternaria panax1, A. alternata2, A. burnsii3, A. rosae4, F. sarcochroum5, F. torreyae6, F. avenaceum7, and F. tricinctum8.

177x160mm (300 x 300 DPI)

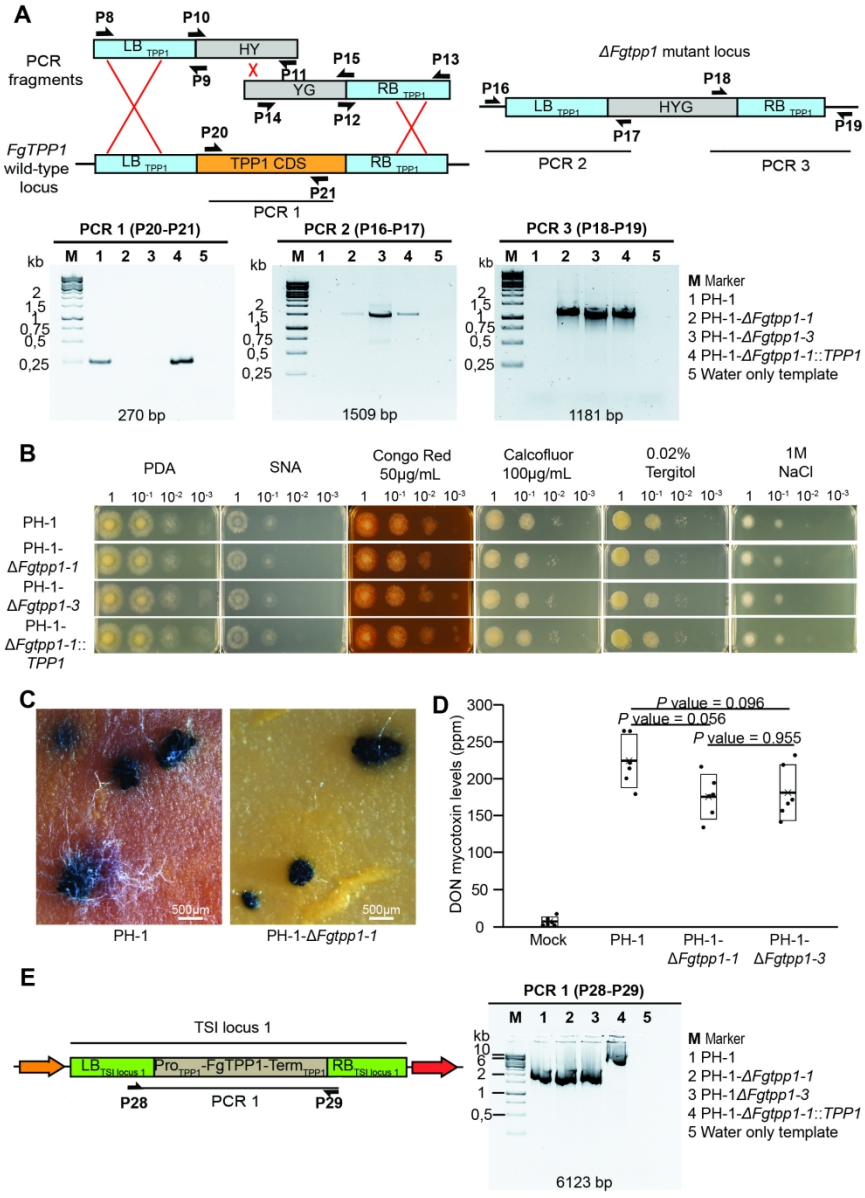

Supplementary Figure S1. In vitro stress tests and DON quantification for wild-type F. graminearum PH-1 strain, the ΔFgtpp1 mutant strains (PH-1-ΔFgtpp1-1 and PH-1-ΔFgtpp1-3, and the complementation strain (PH-1-ΔFgtpp1-1::TPP1). A, The wild-type F. graminearum PH-1 strain was transformed with two PCR fragments containing overlapping sequences of the Hygromycin cassette. Selection of positive transformants was done by multiple PCR amplifications using various primer combinations. Two independent fungal strains were selected in which the FgTPP1 gene had been successfully deleted. PCR 1 (primer combination P20 and P21) evaluated the FgTPP1 coding sequence deletion. PCR2 (primer combination P16 and P17) and PCR3 (primer combination P18 and P19) confirmed correct insertion of the Hygromycin cassette into the FgTPP1 locus. B, Stress tests for wild-type F. graminearum PH-1 strain, both ΔFgtpp1 mutants, and the ΔFgtpp1 complementation strain. The mutant and the complementation strains showed growth rates and morphology indistinguishable from that of the wild-type F. graminearum PH-1 strain for all the conditions evaluated. Images were taken 2 days post-plating on plates. PDA, Potato dextrose agar; SNA, Synthetic nutrient agar; Membrane stresses: Congo Red, Calcofluor, and Tergitol; and salt stress (NaCl). The experiment was repeated twice. C, No obvious defects were observed in perithecia induction and formation between the PH-

1-ΔFgtpp1-1 mutant and the wild-type F. graminearum PH-1 strain. Perithecia images were taken 9 days after perithecia induction on carrot agar medium. D, No statistically significant differences in DON mycotoxin production were observed between the ΔFgtpp1 mutants and wild-type PH-1 strain. DON quantification was performed using wheat spikes infected with either PH-1-ΔFgtpp1-1, PH-1-ΔFgtpp1-3 mutants or the wild-type PH-1 strain. The experiment was repeated twice. Mock inoculated spikes were used as negative control. Data represent the mean of two replicates and error bars denote the 95 % confidence interval (ANOVA followed by Tukey post-hoc test, p value < 0.05). E, Diagnostic PCR for the ΔFgtpp1 complementation strain (PH-1-ΔFgtpp1-1::TPP1). Complementation of the ΔFgtpp1-1 mutant strain was done by integration of a cassette containing a wild-type copy of the FgTPP1 gene including its promoter and terminator into the TSI locus 1. A PCR was performed using primer combination P28 - P29 to evaluate correct insertion of the TPP1 expression cassette containing the TPP1 coding sequence and its native promoter and terminator in the TSI locus 1. PH-1 and the ΔFgtpp1 mutant strains showed a 2100 base pair amplicon whilst the complementation strain showed an amplicon of 6123 base pair, which indicated insertion of the TPP1 cassette in the TSI locus 1.

183x244mm (300 x 300 DPI)

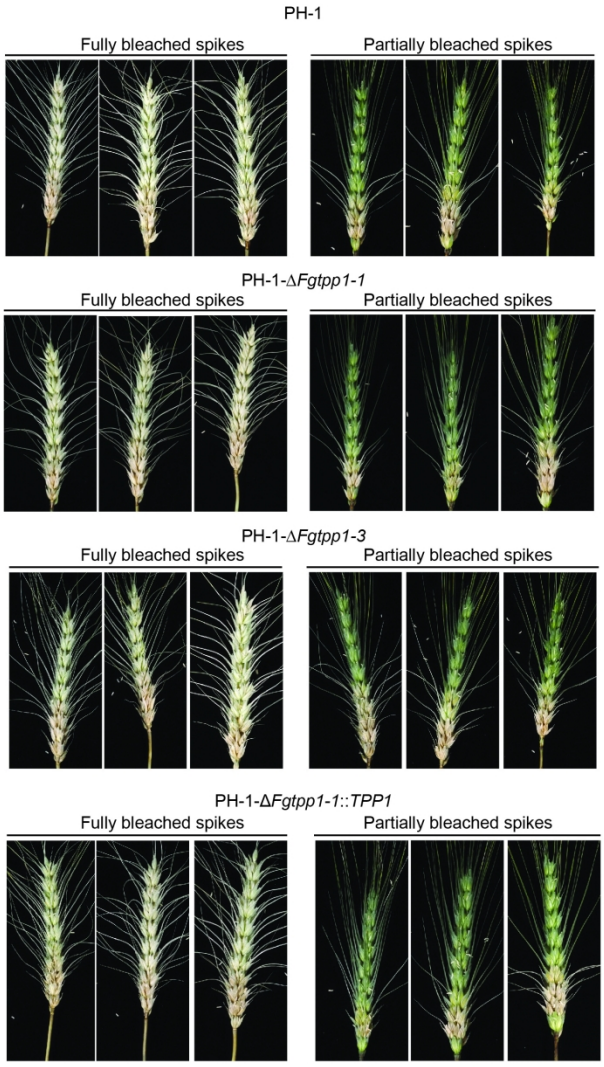

Supplementary Figure S2. Representative images of infected wheat spikes using the bottom inoculation method photographed 10 days post-infection. Images belong to a single replicate where wild-type F. graminearum PH-1, the ΔFgtpp1 mutant strains (PH-1-ΔFgtpp1-1 and PH-1-ΔFgtpp1-3), and the complementation strain (PH-1-ΔFgtpp1-1::TPP1) were evaluated.

177x246mm (300 x 300 DPI)

Supplementary Table S1. Accession numbers for the different *F. graminearum* strains included in the FgTPP1 nucleotide and protein haplotype analyses.

Strain name	Country of origin	Geographic location	Year isolated	NCBI project accession number
PH-1	USA	N/A	2000	PRJNA13839
KSU23473	USA	Georgetown, Minnessota	2000	PRJNA989623
KSU23522	USA	Borup, Minnessota	2000	PRJNA989623
KSU23468	USA	Park river, North Dakota	1999	PRJNA989623
KSU23389	USA	Willsboro, New York	2013	PRJNA989623
NRRL 29169	USA	Kansas	1990	PRJNA527821
233423	USA	Kansas	1995	PRJNA274567
DAOM 241165	Canada	Manitoba	2004	PRJNA274567
CML3066	Brazil	Ijuí, Rio Grande do Sul.	2009	PRJEB12819
CS3005	Australia	Warwick, Queensland	2000	PRJNA235346
N4_2	Germany	Uelzen, Lower Saxony	2016	PRJNA677929
ITA_285	Italy	Italy	1993	PRJNA677929
ITA_1601	Italy	Italy	2001	PRJNA677929
ITA_202	Italy	Italy	1993	PRJNA677929
CBS 119799	South Africa	South Africa	1987	PRJNA677929
CBS 128539	Belgium	Belgium	2007	PRJNA677929
CBS 110263	Iran	Iran	1968	PRJNA677929
114-2	Argentina	Lobera, Province of Cordoba.	2012	PRJNA677929
C10a	France	Chartres, Eure-et-Loir	2002	PRJNA677929
87-7	Argentina	Azul, Province of Buenos Aires	2011	PRJNA677929
S5A	France	Cappelle-en-Pévéle, Nord	2008	PRJNA677929
14C1	Netherlands	Hank, North Brabant	2000	PRJNA677929
0343	Poland	Krzemienica, Gmina Czarna	2003	PRJNA677929
58918	Russia	Krasnodar	2015	PRJNA677929
S17-12	Poland	Braniewo, Warmia	2017	PRJNA677929
Fg820	Netherlands	Zuid Flevoland	1999	PRJNA677929
237	Luxembourg	Luxembourg	2007	PRJNA677929
FG_08	Germany	Bad Schonborn, Baden-Württemberg	1987	PRJNA677929

Supplementary Table S2. FgTPP1 protein homologs in the *Fusarium* genus

Accession number[1]	Fungal species	Fusarium species complex[2]	Lifestyle	Query Coverage	Identity (%)
PTD08981.1	*F. culmorum*	*Sambucinum*	Plant pathogen	100%	99.21
QPC80189.1	*F. pseudograminearum*	*Sambucinum*	Plant pathogen	100%	98.41
CAG7557414.1	*F. equiseti*	*Incarnatum - equiseti*	Plant pathogen	90%	87.72
XP_025594206.1	*F. venenatum*	*Sambucinum*	Plant pathogen	91%	86.15
RGP69575.1	*F. sporotrichioides*	*Sambucinum*	Plant pathogen	100%	86.11
KPA36746.1	*F. langsethiae*	*Sambucinum*	Plant pathogen	100%	86.11
XP_044706991.1	*F. poae*	*Sambucinum*	Plant pathogen	100%	82.14
RGP78819.1	*F. longipes*	*Sambucinum*	Plant endophytic	99%	81.27
XP_046051778.1	*F. redolens*	*Redolens*	Plant pathogen	91%	78.35
KAH7250910.1	*F. tricinctum*	*Tricinctum*	Plant pathogen	91%	76.62
KAJ4249121.1	*F. torreyae*	No complex assigned	Plant pathogen	100%	76.59
KAF4952398.1	*F. sarcochroum*	*Lateritium*	Not known	91%	76.19
KAF4945269.1	*F. gaditjirri*	*Nisikadoi*	Not known	91%	76.19
KAG5655603.1	*F. avenaceum*	*Tricinctum*	Plant pathogen	91%	76.19
XP_018760148.1	*F.verticillioides* 7600	*Fujikuroi*	Plant pathogen	91%	75.76
XP_031031185.1	*F. oxysporum* Fo47	*Oxysporum*	Plant endophytic	91%	75.76
RYC87346.1	*F. oxysporum* f. sp. *narcissi*	*Oxysporum*	Plant pathogen	91%	75.76
EGU81637.1	*F. oxysporum* f. sp. *conglutinans* Fo5176	*Oxysporum*	Plant pathogen	91%	75.76
KAH7245353.1	*F. tricinctum*	*Tricinctum*	Plant pathogen	99%	75.6
KAF4998722.1	*F. graminum*	*Heterosporum*	Not known	100%	75.4
SCV32335.1	*F. fujikuroi*	*Fujikuroi*	Plant pathogen	91%	75.32
RBR01797.1	*F. verticillioides*	*Fujikuroi*	Plant pathogen	91%	75.32
XP_018252424.1	*F. oxysporum* f. sp. *lycopersici* 4287	*Oxysporum*	Plant pathogen	91%	75.32
KAF4341936.1	*F. beomiforme*	*Babinda*	not known	91%	74.89

KAG5750526.1	*F. xylarioides*	*Fujikuroi*	Plant pathogen	91%	74.89
XP_041677642.1	*F. mangiferae*	*Fujikuroi*	Plant pathogen	91%	74.89
KAF5689528.1	*F. circinatum*	*Fujikuroi*	Plant pathogen	91%	74.89
XP_036533940.1	*F. subglutinans*	*Fujikuroi*	Plant pathogen	91%	74.46
SPJ76027.1	*F. torulosum*	*Tricinctum*	Not known	99%	74.4
KAG5659696.1	*F. avenaceum*	*Tricinctum*	Plant pathogen	99%	74.4
KAF5667294.1	*F. heterosporum*	*Heterosporum*	hyperparasite of *Claviceps purpurea*	100%	73.81
KAF4947933.1	*F. sarcochroum*	*Lateritium*	Not known	99%	71.37
KAJ4252383.1	*F. torreyae*	No complex assigned	Plant pathogen	95%	70.04

[1] The presence of a secretion signal and a chloroplast transit peptide were predicted using SignalP v6.0 (Teufel et al. 2022) and LOCALIZER v1.0 (Sperschneider et al. 2017), respectively. All proteins showed probability values above 0.99 and 0.95 for the presence of a secretion signal and chloroplast transit peptide sequences, respectively.

[2] *Fusarium* species were assigned to the different *Fusarium* species complexes based on the classification done by Waalwijk et al (2018).

Supplementary Table S3. Estimates of evolutionary divergence between 28 TPP1 sequences (dN/dS).

	PH-1	14C1	87-7	114-2	237	0343	Fg820	58918	C10a	CBS_110263	CBS_2_128539	CML3066	CS3005	DAOM_241165	233423	FG_08	ITA-285	ITA_202	ITA_1601	KSU23389	KSU23468	KSU23473	KSU23522	N4_2	NRRL_29169	S5A	S17-12	CBS_3_119799
PH-1		0.001856	0.001856	0.001369	0.003745	0.001369	0.001369	0.001856	0.001903	0.001369	0.003745	0.001856	0.001369	0.001369	0.001369	0.001369	0.001369	0.001369	0.001369	0.001856	0.000000	0.001908	0.002423	0.001369	0.001856	0.001369	0.003745	0.001369	0.001369
14C1	0.002654		0.000000	0.001285	0.003681	0.001285	0.001285	0.000000	0.001843	0.001285	0.003681	0.000000	0.001285	0.001285	0.001285	0.001285	0.001285	0.001285	0.000000	0.001856	0.001853	0.002284	0.001285	0.000000	0.001285	0.003681	0.001285	0.001285
87-7	0.002654	0.000000		0.001285	0.003681	0.001285	0.001285	0.000000	0.001843	0.001285	0.003681	0.000000	0.001285	0.001285	0.001285	0.001285	0.001285	0.001285	0.000000	0.001856	0.001853	0.002284	0.001285	0.000000	0.001285	0.003681	0.001285	0.001285
114-2	0.001327	0.001324	0.001324		0.003430	0.000000	0.000000	0.001285	0.001231	0.000000	0.003430	0.001285	0.000000	0.000000	0.000000	0.000000	0.000000	0.000000	0.001285	0.001369	0.001360	0.001960	0.000000	0.001285	0.000000	0.003430	0.000000	0.000000
237	0.003351	0.003356	0.003356	0.008022		0.003430	0.003430	0.003681	0.003199	0.003430	0.000000	0.003681	0.003430	0.003430	0.003430	0.003430	0.003430	0.003430	0.003681	0.003745	0.003706	0.004005	0.003430	0.003681	0.003430	0.000000	0.003430	0.003430
0343	0.001327	0.001324	0.001324	0.000000	0.008022		0.000000	0.001285	0.001231	0.000000	0.003430	0.001285	0.000000	0.000000	0.000000	0.000000	0.000000	0.000000	0.001285	0.001369	0.001360	0.001960	0.000000	0.001285	0.000000	0.003430	0.000000	0.000000
Fg820	0.001327	0.001324	0.001324	0.000000	0.008022	0.000000		0.001285	0.001231	0.000000	0.003430	0.001285	0.000000	0.000000	0.000000	0.000000	0.000000	0.000000	0.001285	0.001369	0.001360	0.001960	0.000000	0.001285	0.000000	0.003430	0.000000	0.000000
58918	0.002654	0.000000	0.000000	0.001324	0.003356	0.001324	0.001324		0.001843	0.001285	0.003681	0.000000	0.001285	0.001285	0.001285	0.001285	0.001285	0.001285	0.000000	0.001856	0.001853	0.002284	0.001285	0.000000	0.001285	0.003681	0.001285	0.001285
C10a	0.002654	0.002651	0.002651	0.001324	0.006630	0.001324	0.001324	0.002651		0.001231	0.003199	0.001843	0.001231	0.001231	0.001231	0.001231	0.001231	0.001231	0.001843	0.001903	0.001849	0.002344	0.001231	0.001843	0.001231	0.003199	0.001231	0.001231
CBS_110263	0.001327	0.001324	0.001324	0.000000	0.008022	0.000000	0.000000	0.001324	0.001324		0.003430	0.001285	0.000000	0.000000	0.000000	0.000000	0.000000	0.000000	0.001285	0.001369	0.001360	0.001960	0.000000	0.001285	0.000000	0.003430	0.000000	0.000000
CBS_2_128539	0.003351	0.003356	0.003356	0.008022	0.000000	0.008022	0.008022	0.003356	0.006630	0.008022		0.003681	0.003430	0.003430	0.003430	0.003430	0.003430	0.003430	0.003681	0.003745	0.003706	0.004005	0.003430	0.003681	0.003430	0.000000	0.003430	0.003430
CML3066	0.002654	0.000000	0.000000	0.001324	0.003356	0.001324	0.001324	0.000000	0.002651	0.001324	0.003356		0.001285	0.001285	0.001285	0.001285	0.001285	0.001285	0.000000	0.001856	0.001853	0.002284	0.001285	0.000000	0.001285	0.003681	0.001285	0.001285
CS3005	0.001327	0.001324	0.001324	0.000000	0.008022	0.000000	0.000000	0.001324	0.001324	0.000000	0.008022	0.001324		0.000000	0.000000	0.000000	0.000000	0.000000	0.001285	0.001369	0.001360	0.001960	0.000000	0.001285	0.000000	0.003430	0.000000	0.000000
DAOM_241165	0.001327	0.001324	0.001324	0.000000	0.008022	0.000000	0.000000	0.001324	0.001324	0.000000	0.008022	0.001324	0.000000		0.000000	0.000000	0.000000	0.000000	0.001285	0.001369	0.001360	0.001960	0.000000	0.001285	0.000000	0.003430	0.000000	0.000000
233423	0.001327	0.001324	0.001324	0.000000	0.008022	0.000000	0.000000	0.001324	0.001324	0.000000	0.008022	0.001324	0.000000	0.000000		0.000000	0.000000	0.000000	0.001285	0.001369	0.001360	0.001960	0.000000	0.001285	0.000000	0.003430	0.000000	0.000000
FG_08	0.001327	0.001324	0.001324	0.000000	0.008022	0.000000	0.000000	0.001324	0.001324	0.000000	0.008022	0.001324	0.000000	0.000000	0.000000		0.000000	0.000000	0.001285	0.001369	0.001360	0.001960	0.000000	0.001285	0.000000	0.003430	0.000000	0.000000
ITA-285	0.001327	0.001324	0.001324	0.000000	0.008022	0.000000	0.000000	0.001324	0.001324	0.000000	0.008022	0.001324	0.000000	0.000000	0.000000	0.000000		0.000000	0.001285	0.001369	0.001360	0.001960	0.000000	0.001285	0.000000	0.003430	0.000000	0.000000
ITA_202	0.001327	0.001324	0.001324	0.000000	0.008022	0.000000	0.000000	0.001324	0.001324	0.000000	0.008022	0.001324	0.000000	0.000000	0.000000	0.000000	0.000000		0.001285	0.001369	0.001360	0.001960	0.000000	0.001285	0.000000	0.003430	0.000000	0.000000
ITA_1601	0.002654	0.000000	0.000000	0.001324	0.003356	0.001324	0.001324	0.000000	0.002651	0.001324	0.003356	0.000000	0.001324	0.001324	0.001324	0.001324	0.001324	0.001324		0.001856	0.001853	0.002284	0.001285	0.000000	0.001285	0.003681	0.001285	0.001285
KSU23389	0.000000	0.002654	0.002654	0.001327	0.003351	0.001327	0.001327	0.002654	0.002654	0.001327	0.003351	0.002654	0.001327	0.001327	0.001327	0.001327	0.001327	0.001327	0.002654		0.001908	0.002423	0.001369	0.001856	0.001369	0.003745	0.001369	0.001369
KSU23468	0.002654	0.002651	0.002651	0.001324	0.003356	0.001324	0.001324	0.002651	0.002651	0.001324	0.003356	0.002651	0.001324	0.001324	0.001324	0.001324	0.001324	0.001324	0.002651	0.002654		0.002432	0.001360	0.001853	0.001360	0.003706	0.001360	0.001360
KSU23473	0.003985	0.003985	0.003985	0.002658	0.010744	0.002658	0.002658	0.003985	0.003985	0.002658	0.010744	0.003985	0.002658	0.002658	0.002658	0.002658	0.002658	0.002658	0.003985	0.003985	0.003985		0.001960	0.002284	0.001960	0.004005	0.001960	0.001960
KSU23522	0.001327	0.001324	0.001324	0.000000	0.008022	0.000000	0.000000	0.001324	0.001324	0.000000	0.008022	0.001324	0.000000	0.000000	0.000000	0.000000	0.000000	0.000000	0.001324	0.001327	0.001324	0.002658		0.001285	0.000000	0.003430	0.000000	0.000000
N4_2	0.002654	0.000000	0.000000	0.001324	0.003356	0.001324	0.001324	0.000000	0.002651	0.001324	0.003356	0.000000	0.001324	0.001324	0.001324	0.001324	0.001324	0.001324	0.000000	0.002654	0.002651	0.003985	0.001324		0.001285	0.003681	0.001285	0.001285
NRRL_29169	0.001327	0.001324	0.001324	0.000000	0.008022	0.000000	0.000000	0.001324	0.001324	0.000000	0.008022	0.001324	0.000000	0.000000	0.000000	0.000000	0.000000	0.000000	0.001324	0.001327	0.001324	0.002658	0.000000	0.001324		0.003430	0.000000	0.000000
S5A	0.003351	0.003356	0.003356	0.008022	0.000000	0.008022	0.008022	0.003356	0.006630	0.008022	0.000000	0.003356	0.008022	0.008022	0.008022	0.008022	0.008022	0.008022	0.003356	0.003351	0.003356	0.010744	0.008022	0.003356	0.008022		0.003430	0.003430
S17-12	0.001327	0.001324	0.001324	0.000000	0.008022	0.000000	0.000000	0.001324	0.001324	0.000000	0.008022	0.001324	0.000000	0.000000	0.000000	0.000000	0.000000	0.000000	0.001324	0.001327	0.001324	0.002658	0.000000	0.001324	0.000000	0.008022		0.000000
CBS_3_119799	0.001327	0.001324	0.001324	0.000000	0.008022	0.000000	0.000000	0.001324	0.001324	0.000000	0.008022	0.001324	0.000000	0.000000	0.000000	0.000000	0.000000	0.000000	0.001324	0.001327	0.001324	0.002658	0.000000	0.001324	0.000000	0.008022	0.000000	

The number of base substitutions per site from between sequences are shown. Standard error estimate(s) are shown above the diagonal. Analyses were conducted using the Tamura-Nei model. This analysis involved 28 nucleotide TPP1 sequences. Codon positions included were 1st + 2nd +3rd and noncoding. All ambiguous positions were removed for each sequence pair (pairwise deletion option). There was a total of 759 positions in the final dataset. Evolutionary analyses were done using MEGA11.

Supplementary Table S4. FgTPP1 protein homologs in different genera of the *Ascomycota* phylum

Accession number[1]	Fungal species	Order	Lifestyle	Query Coverage	Percent Identity
XP_033446225.1	*Didymella exigua* CBS 183.55	Pleosporales	plant pathogenic	97%	64.08
KAH7141753.1	*Dactylonectria macrodidyma*	Hypocreales	endophytic	99%	63.39
KAH7089434.1	*Paraphoma chrysanthemicola*	Pleosporales	endophytic	89%	63.04
XP_046026864.1	*Alternaria rosae*	Pleosporales	endophytic	92%	63.03
XP_018389683.1	*Alternaria alternata*	Pleosporales	plant pathogenic	92%	63.03
XP_038791682.1	*Alternaria burnsii*	Pleosporales	plant pathogenic	92%	62.61
KAH7074004.1	*Paraphoma chrysanthemicola*	Pleosporales	endophytic	89%	62.61
KAF4552574.1	*Elsinoe fawcettii*	Myriangiales	plant pathogenic	100%	62.45
KXJ86523.1	*Microdochium bolleyi*	Xylariales	endophytic	89%	61.84
KPM41428.1	*Neonectria ditissima*	Hypocreales	plant pathogenic	88%	61.5
KZL65301.1	*Colletotrichum tofieldiae*	Glomerellales	endophytic	96%	61.48
KAH7375564.1	*Plectosphaerella cucumerina*	Glomerellales	endophytic	97%	60.32
KAI9152319.1	*Paramyrothecium foliicola*	Hypocreales	plant pathogenic	89%	60.18
KAJ4985316.1	*Stagonosporopsis vannaccii*	Pleosporales	plant pathogenic	97%	59.35
KAF1917785.1	*Ampelomyces quisqualis*	Pleosporales	hyperparasite of powdery mildew fungi	97%	59.23
KAH7304750.1	*Stachybotrys elegans*	Hypocreales	endophytic	91%	58.87
KAG9192201.1	*Alternaria panax*	Pleosporales	plant pathogenic	97%	58.85
KNG47033.1	*Stemphylium lycopersici*	Pleosporales	plant pathogenic	98%	58.78
KKY36680.1	*Diaporthe ampelina*	Diaporthales	plant pathogenic	89%	58.67
KAF9732810.1	*Paraphaeosphaeria minitans*	Pleosporales	biocontrol	90%	58.26

XP_003002233.1	*Verticillium alfalfae* VaMs.102	Glomerellales	plant pathogenic	96%	58.02
KAH7073840.1	*Paraphoma chrysanthemicola*	Pleosporales	endophytic	97%	57.87
RMZ73582.1	*Pyrenophora seminiperda* CCB06	Pleosporales	plant pathogenic	90%	57.87
KAH7175313.1	*Dactylonectria macrodidyma*	Hypocreales	endophytic	98%	57.81
USP77425.1	*Curvularia clavata*	Pleosporales	plant pathogenic	98%	57.65
XP_009653342.1	*Verticillium dahliae* VdLs.17	Glomerellales	plant pathogenic	96%	57.61
KAH7089599.1	*Paraphoma chrysanthemicola*	Pleosporales	endophytic	97%	57.48
PVH94868.1	*Periconia macrospinosa*	Pleosporales	endophytic	89%	57.27
XP_046013457.1	*Microdochium trichocladiopsis*	Xylariales	endophytic	99%	56.81
XP_038793509.1	*Ascochyta rabiei*	Pleosporales	plant pathogenic	99%	56.35
XP_038784058.1	*Alternaria burnsii*	Pleosporales	plant pathogenic	97%	56.32
KAF9740106.1	*Paraphaeosphaeria minitans*	Pleosporales	mycoparasite of Sclerotinia/biocontrol	99%	56.06
XP_018386207.1	*Alternaria alternata*	Pleosporales	plant pathogenic	97%	55.94
XP_046106460.1	*Ilyonectria robusta*	Hypocreales	endophytic	99%	55.56
KAG9192130.1	*Alternaria panax*	Pleosporales	plant pathogenic	98%	55.51
GKT86035.1	*Colletotrichum tofieldiae*	Glomerellales	endophytic	99%	55.2
XP_046025926.1	*Alternaria rosae*	Pleosporales	endophytic	98%	55.13
XP_038791744.1	*Alternaria burnsii*	Pleosporales	plant pathogenic	98%	54.37
XP_018389611.1	*Alternaria alternata*	Pleosporales	plant pathogenic	98%	53.99
XP_038800935.1	*Ascochyta rabiei*	Pleosporales	plant pathogenic	94%	53.23
XP_056027974.1	*Trichoderma breve*	Hypocreales	biocontrol	98%	53.01
KKP04050.1	*Trichoderma harzianum*	Hypocreales	biocontrol	99%	52.76
KAH7322444.1	*Stachybotrys elegans*	Hypocreales	endophytic	99%	51.97
KNG51985.1	*Stemphylium lycopersici*	Pleosporales	plant pathogenic	98%	51.91

[1] The presence of a secretion signal and a chloroplast transit peptide were predicted using SignalP v6.0 (Teufel et al. 2022) and LOCALIZER (Sperschneider et al. 2017), respectively. All the proteins showed probabilities values above 0.99 and 0.80 for the presence of a secretion signal and chloroplast transit peptide sequences, respectively.

Supplementary Table S5. List of primers used in this work.

Primer	Name	5'-3' Sequence	Purpose
P1	TPP1_attB1_F	GGGGACAAGTTTGTACAAAAAAGCAGGCTTCATGGTCAAGATCACTTC	Yeast trap assay
P2	TPP1_attB2_R	GGGGACCACTTTGTACAAGAAAGCTGGGTCGGCGTTGCTGTCGATC	Yeast trap assay
P3	OSP24_attB1_F	GGGGACAAGTTTGTACAAAAAAGCAGGCTTCATGCGCTACCTCCAAAACAT	Yeast trap assay
P4	OSP24_attB2_R	GGGGACCACTTTGTACAAGAAAGCTGGGTCCAAGCTCGAGCGGTAGCAAAG	Yeast trap assay
P5	TPP1$^{\Delta SP}$_attB1_F	GGGGACAAGTTTGTACAAAAAAGCAGGCTTCATGGCTCCCAACCCTCAGA	Yeast trap assay
P6	ADH1_F	CGGTATACGGCCTTCCTTCC	Yeast trap assay
P7	SUC_R	TTGGGTCATTCATCCAGCCC	Yeast trap assay
P8	EK101_TPP1_F	ccgcgggaattcgatCATAAACTCCTGCCTTGTC	P_{TPP1} (TPP1 left border)
P9	EK102_TPP1_R	gttatcgaatTGTGACGAAGTAGGAGTTATC	P_{TPP1} (TPP1 left border)
P10	EK103_Hyg$_{1-761}$_F	tcgtcacaATTCGATAACTGATATTGAAGGAGCATTTTTT	HyG expression cassette fragment (Hyg$_{1-761}$)
P11	U653_ Hyg$_{1-761}$_R	gccgcgaattcactagtgatGGATGCCTCCGCTCGAAG	HyG expression cassette fragment (Hyg$_{1-761}$)
P12	EK28_TPP1_F	cgacctcgagACATCATAAACTGTTTAGTGATTTTG	T_{TPP1} (TPP1 right border)
P13	EK29_TPP1_R	gccgcgaattcactagtgatCATGCGCTTTGATCTTGC	T_{TPP1} (TPP1 right border)
P14	EK27_Hyg$_{296-1027}$_F	tttatgatgtCTCGAGGTCGACGGTATC	HyG expression cassette fragment (Hyg$_{296-1027}$)
P15	U654_Hyg$_{296-1027}$_R	ccgcgggaattcgatCGTTGCAAGACCTGCCTG	HyG expression cassette fragment (Hyg$_{296-1027}$)
P16	EK46_TPP1_7F	GCAGAAGGCCTCTTTAATTG	LB border of ΔTPP1 gene
P17	U667_HYG1_R	ACTTCTCGACAGACGTCGC	LB border of ΔTPP1 gene
P18	U668_HYG2_F	TGGCTGTGTAGAAGTACTCG	2nd border diagnostic
P19	EK33_TPP1_8R	TTCGACAATCGCCCGATGAT	2nd border diagnostic
P20	TPP1_qPCR_R1	GGCAGGGATGGAAGTGGAAA	TPP1 coding sequence replacement
P21	TPP1_qPCR_F2	GCGGTGGTACTCTCCTCAAC	TPP1 coding sequence replacement
P22	RD3_TPP1_F	GGGATATGGTCTCAACCTGAGCGATTTCCACAGACGAT	TPP1 complementation
P23	RD4_TPP1_R	CCCATATGGTCTCGTAGTGATCAGTACTAAAGTATCCA	TPP1 complementation
P24	P3[1]	TATGCTCTTCAACACGATGTCCTGGTAGCGATCC	To amplify *geneticin*$_{1-664}$-P_{TPP1}-TPP1-T_{TPP1}-RB
P25	P4[1]	TATGCTCTTCATGACCAGAACCACCAATAACTG	To amplify *geneticin*$_{1-664}$-P_{TPP1}-TPP1-T_{TPP1}-RB
P26	P1[1]	ATATCTCGAGGTCTCCTTTAATC	To amplify LB-*geneticin*$_{795-128}$

P27	P2[1]	ATATCTCGAGCCGACCAGTCC	To amplify LB-*geneticin*$_{795\text{-}128}$
P28	P5[1]	TGCTACAGACAAAACCCGCT	To check correct insertion of the cassette into TSI locus 1
P29	P10[1]	AGATGGACTCCCGGACATCA	To check correct insertion of the cassette into TSI locus 1
P30	FgTPP1_F w/o SP	TATGGTCTCAGGCTGTATGGCTCCCAACCCTCAGAAC	TPP1 open reading frame for Golden Gate cloning
P31	FgTPP1_R	TATGGTCTCACTGAGGCGTTGCTGTCGATCCAAG	TPP1 open reading frame for Golden Gate cloning

[1] Primers sequences were extracted from Darino et al. (2024).